https://ntrs.nasa.gov/search.jsp?R=19810015205 2020-03-21T13:50:02+00:00Z

N O T I C E

THIS DOCUMENT HAS BEEN REPRODUCED FROM MICROFICHE. ALTHOUGH IT IS RECOGNIZED THAT CERTAIN PORTIONS ARE ILLEGIBLE, IT IS BEING RELEASED IN THE INTEREST OF MAKING AVAILABLE AS MUCH INFORMATION AS POSSIBLE

THE CTS 11.7 GHz ANGLE OF ARRIVAL EXPERIMENT

B.W. Kwan and D.B. Hodge

Technical Report 712759-2
January 1981
Contract NASW-3393

(NASA-CR-164338) THE CTS 11.7 GHz ANGLE OF ARRIVAL EXPERIMENT Interim Report (Ohio State Univ., Columbus.) 63 p HC A04/MF A01 CSCL 04A

N81-23740

Unclas
G3/46 15005

National Aeronautics and Space Administration Headquarters
Washington, D.C. 20546

TABLE OF CONTENTS

	Page
LIST OF TABLES	iv
LIST OF FIGURES	v
I. INTRODUCTION	1
II. THE EXPERIMENT	3
Receiving System	5
1. Antenna	5
2. The Four Phase Lock Loop Receivers	5
Amplitude calibration scheme	11
Phase calibration scheme	11
3. The Digital System	15
III. DATA ANALYSIS	15
Projection Algorithm	27
IV. RESULTS	28
Attenuation Statistics	37
Differential Phase Statistics	47
V. RAIN RATE	54
VI. DISCUSSION	54
REFERENCES	57

PRECEDING PAGE BLANK-NOT FILMED

LIST OF TABLES

Table		Page
1	CTS BEACON PARAMETERS	6
2	OSU GROUND TERMINAL PARAMETERS	6
3	DOWNLINK MARGIN CALCULATIONS	12
4	TAPE RECORD HEADER FORMAT	19
5	STATUS WORDS - CTS	20
6	REAL-TIME-CLOCK WORDS	21
7	RECORD TYPE 12, 13 FORMAT	22
8	FIXED TERMINAL CHANNEL ASSIGNMENTS - CTS	23
9	SUMMARY OF CTS ANGLE OF ARRIVAL DATA PERIODS	24

LIST OF FIGURES

Figure		Page
1	A simplified view of the CTS angle of arrival experiment	2
2	A plane wave arriving at an array of the two elements	4
3	Self phased array configuration	7
4	A picture of the four-element self phased array	8
5	Diurnal motion of the spacecraft in the AZ-EL plane superimposed on the pattern contours for a single array element	9
6	Self phased array receiver block diagram	10
7	Test configuration for amplitude calibration	13
8	Average amplitude calibration curve for the four PLL receivers at 11.7 GHz	14
9	Phase calibration curve	16
10	The digital data system configuration	17
11	Tape record format	18
12	Beacon frequency: days 41 and 42, 1977	26
13	Flow chart for computing and projecting reference mean levels	29
14	CTS 11.7 GHz beacon: day 73 13H 18M 47S (1977)	31
15	CTS 11.7 GHz beacon: day 94 18H 43M 3S (1977)	32
16	CTS 11.7 GHz beacon: day 193 21H 58M 58S (1977)	34
17	CTS 11.7 GHz beacon: day 233 19H 2M 25S (1977)	35
18	CTS 11.7 GHz beacon: day 233 19H 2M 25S (1977) - Comparison of array and single element fading	36
19	Cumulative distributions of sum amplitude for May, June, and August, 1976	38
20	Cumulative distributions of sum amplitude for January-June, 1977	39
21	Cumulative distributions of sum amplitude for July-December, 1977	40

		Page
22	Cumulative distributions of sum amplitude for January-June, 1978	41
23	Cumulative distributions of sum amplitude for 1976, 1977, and 1978	42
24	Cumulative distributions of sum amplitude variance for May, June, and August, 1976	43
25	Monthly cumulative distributions of sum amplitude variance for January-December (except September), 1977	44
26	Cumulative distributions of sum amplitude variance for January-June, 1978	45
27	Cumulative distributions of sum amplitude for 1976, 1977, and 1978	46
28	Cumulative distributions of differential phase for May, June, and August, 1976	48
29	Cumulative distributions of differential phase for January-December (except September), 1977	49
30	Cumulative distributions of differential phase for January-June, 1978	50
31	Cumulative distributions of differential phase variance for May, June, and August, 1976	51
32	The cumulative distributions of differential phase variance for January-December (except September, 1977	52
33	Cumulative distributions of differential phase variance for January-June, 1978	53
34	Rain rate distributions for the CTS 11.7 GHz angle of arrival experiment data periods	55
35	Rain rate distributions for 1976, 1977, and 1978	56

I. INTRODUCTION

During the period 1976-1978, The Ohio State University ElectroScience Laboratory participated in the Communications Technology Satellite (CTS) Link Characterization Experiment initiated by NASA/GSFC. The objective of the experiment was to determine the statistical behavior of attenuation and angle of arrival on an earth-space propagation path using the CTS 11.7 GHz beacon. Attenuation is primarily a result of rainfall on the path, while amplitude scintillation and angle of arrival fluctuation can be due to the presence of clouds, turbulence, and/or refractive layers. The existence of significant amplitude scintillation on millimeter wavelength paths, particularly in the presence of nonprecipitating cloud or on low elevation angle paths, has been well established. Angle of arrival fluctuations as large as 0.3^{o} on 35 GHz terrestrial links have been observed [6] ; and measurements at 35 GHz on a 10-km terrestrial path have yielded angle of arrival fluctuations as large as 0.1^{o} [7] . Thus, it would be useful to establish the extent of angle of arrival fluctuations on earth-space paths. On the one hand, it would appear that such fluctuations would be less than those observed on terrestrial links since the distance through the lower troposphere may be shorter; but, on the other hand, the earth-space path must often pass through regions of cloud which would not normally be found on terrestrial paths. Angle of arrival fluctuations ultimately restrict the achievable gain for large aperture antennas and may cause reductions in the coherent bandwidth.

The empirical data obtained during the above period are edited and analyzed. Cumulative distributions on signal attenuation and angle of arrival are constructed. Rainfall rate distributions are also prepared to provide a cumulative comparison of the above two disruptive effects with meteorological data.

The principal elements of the CTS Experiment are shown in Figure 1. The carrier at 11.7 GHz is transmitted from the spacecraft. A four-element self phased array is employed at the earth-based receiving station. The propagation measurements involve five amplitudes (one from

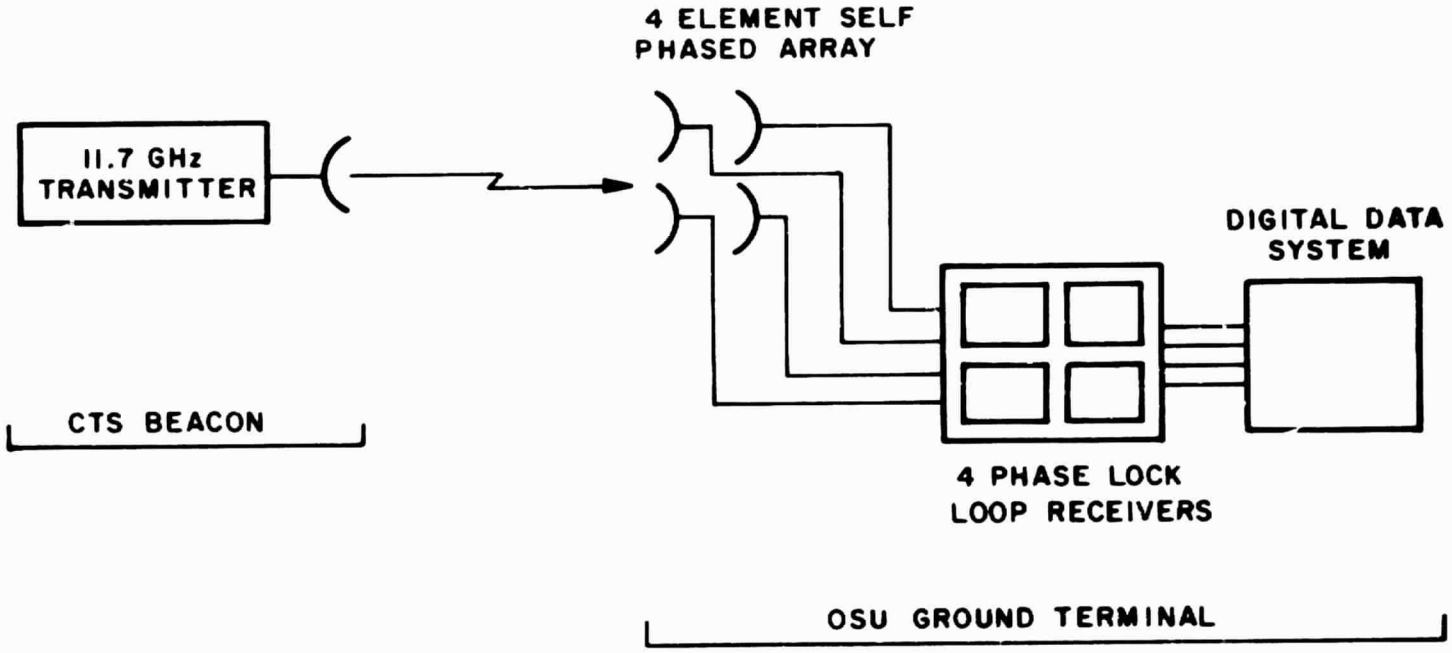

Figure 1. A simplified view of the CTS angle of arrival experiment

each element of its array and their coherent sum) and four differential phases. These differential phases are directly related to the apparent angle of arrival. These measurements are sampled at a rate of 1/3 Hz and converted to digital levels, which are then recorded on magnetic tape. The measurements are fully automated and are made twenty-four hours a day. Detailed descriptions of the overall experiment are given in references [1] and [2]. Essential features of the experiment are repeated in the following section of this report for completeness.

II. THE EXPERIMENT

In this experiment, the notion of apparent angle of arrival is used. This concept is used since only limited phase information is available. In general, one must represent the received signal as a spectrum of plane waves. Nevertheless, the idea of apparent angle of arrival allows one to quantify the observed behavior in a manner which permits simpler interpretation.

Using elementary array theory, if d is the distance between two elements and α is the angle of arrival measured between the axis of the array and the propagation direction of a plane wave (Figure 2), the differential phase between the signals received by the elements is:

$$\Delta\phi = k\Delta z = k\, d \sin\alpha \tag{1}$$

But, for small angles,

$$\sin\alpha \simeq \alpha \tag{2}$$

so,

$$\Delta\phi = 2\pi \frac{d}{\lambda} \alpha \tag{3}$$

Thus, by monitoring the differential phases associated with two orthogonal

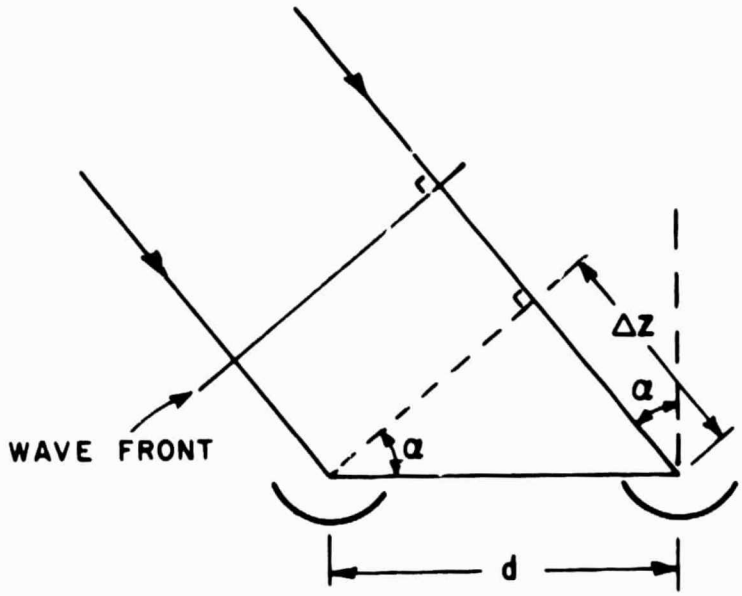

Figure 2. A plane wave arriving at an array of the two elements

pairs of elements of the four-element array, one can obtain the apparent angle of arrival. The differential phases from the remaining pairs can be used to determine the degree to which the incoming signal differs from an ideal plane wave. In this experiment, four phase lock loop receivers are implemented to provide the appropriate differential phases. The array and the receivers will be described in the following sections.

Receiving System

The receiving system consists of the antenna (the four-element array), the four phase lock loop receivers, and the digital data system. The parameters of the CTS beacon and the O.S.U. earth-based station are tabulated in Tables 1 and 2.

1. Antenna

The antenna system consists of a four-element array. Each element is a parabolic reflector with a diameter of 0.6 m. The elements are located at the corners of a planar surface of area one meter square, such that two differential phases in the elevation plane and two differential phases in the azimuth plane can be measured. This spacing is a result of the constraints that the spacing must be large enough to provide reasonable angular resolution and, yet, be small enough to eliminate ambiguity problems associated with large differential phase excursions. The array configuration and the notation used for the measured variables are shown in Figure 3. Figure 4 shows a photograph of the four-element array.

Figure 5 is a plot showing the diurnal motion of the spacecraft in the AZ-EL plane superimposed on the pattern contours of a single element of the receiving array. It is apparent from this plot that the diurnal amplitude variation is less than 1 dB for the fixed array.

2. The Four Phase Lock Loop Receivers

Each receiver (Figure 6) is a modified Collins 75-S3. The phase of the signal from each array element is aligned with that of a reference

TABLE 1

CTS BEACON PARAMETERS

Beacon Type

Operating frequency - 11.7 GHz
Power output - 200 mW

Antenna

Boresight - 20^{o} N, 105^{o} W
Polarization - Right hand circular
Bandwidth - 100 MHz
Gain- > 18.4 dB for $0^{o} < \phi < 5.25^{o}$
> 17.3 dB for $\phi = 7.25^{o}$
> 16.4 dB for $\phi = 8.50^{o}$

TABLE 2

OSU GROUND TERMINAL PARAMETERS

Latitude - 40.0028^{o} N
Longitude - 83.0417^{o}W
Nominal satellite look angles - Azimuth 225.3^{o}
Elevation 32.7^{o}

Antenna: Four-element array

Elements: Parabolic reflectors with focal point feeds
Aperture size - 0.6 m.
Polarization - Right hand circular
Bandwidth - 3^{o}

Receiver: One Collins 75-S3 receiver for each array element modified for PLL operation

Noise figure - 7.0 to 7.2 dB
Data bandwidth - 80 Hz

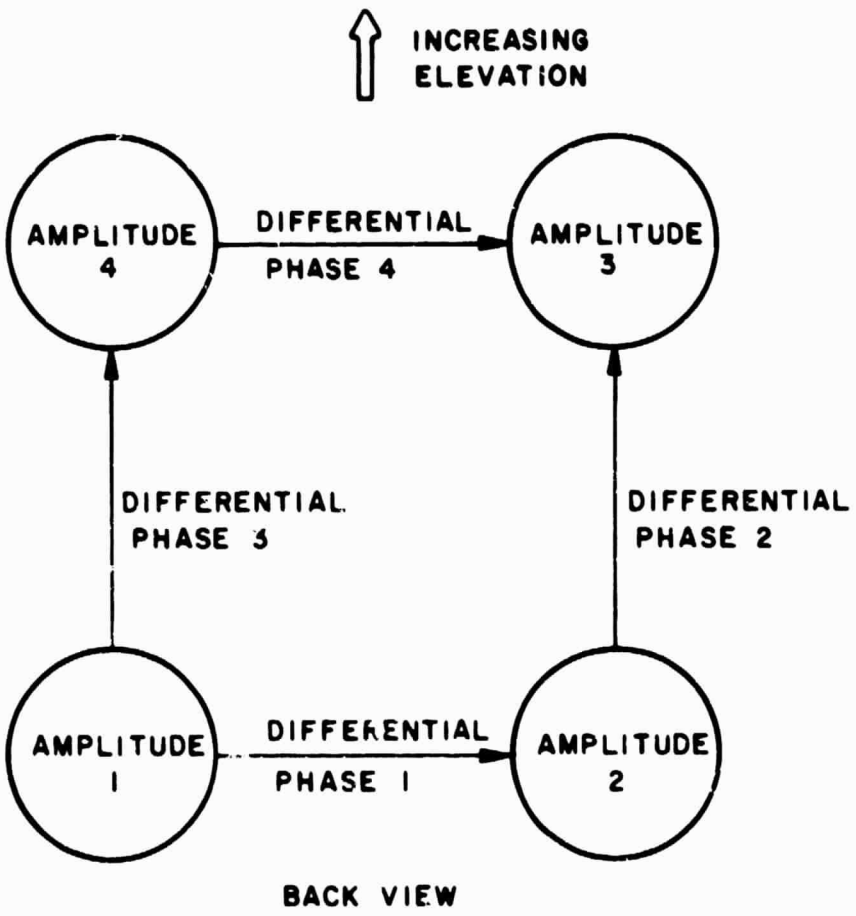

Figure 3. Self phased array configuration

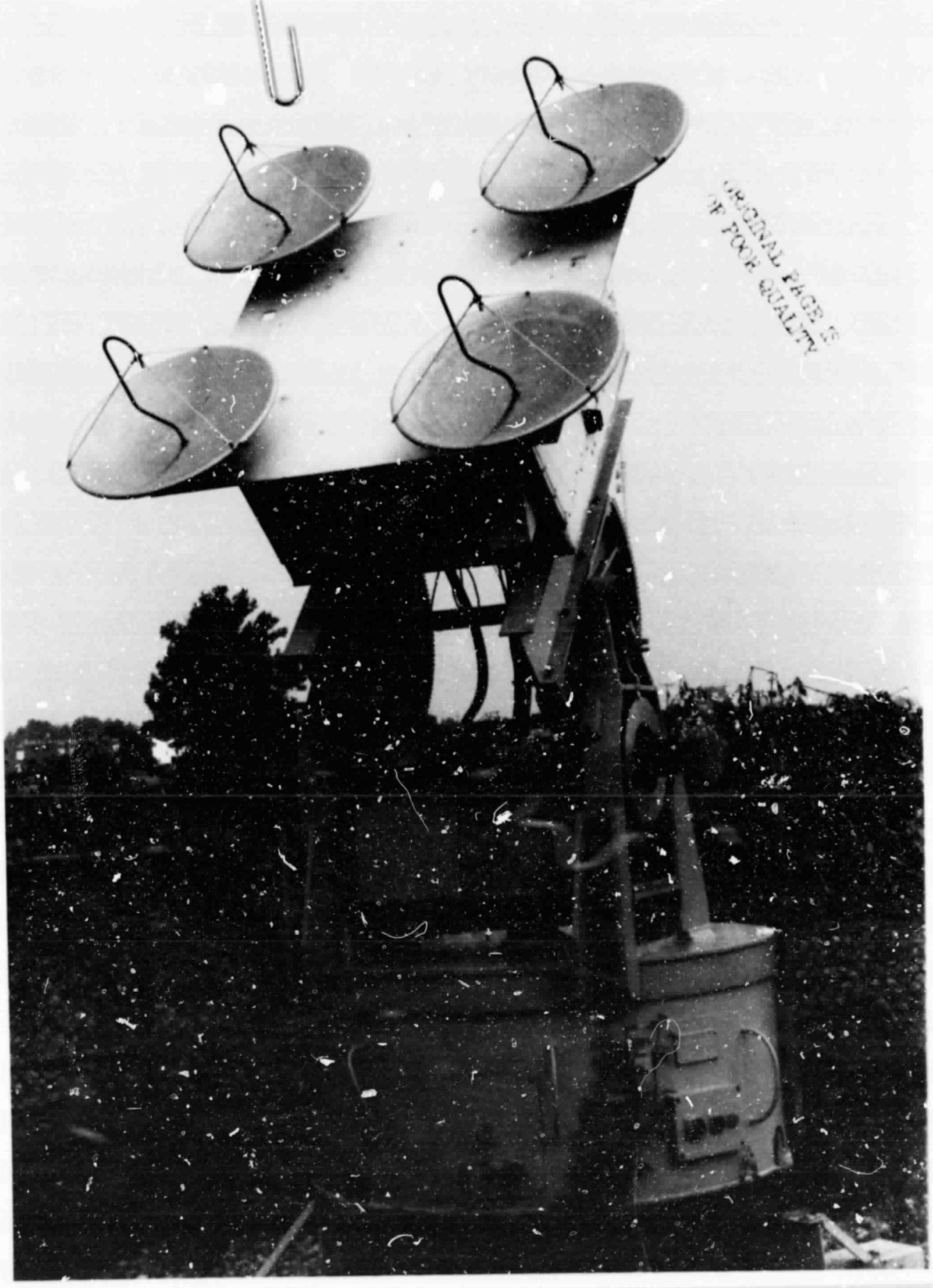
ORIGINAL PAGE IS
OF POOR QUALITY

Figure 4. A picture of the four-element self phased array

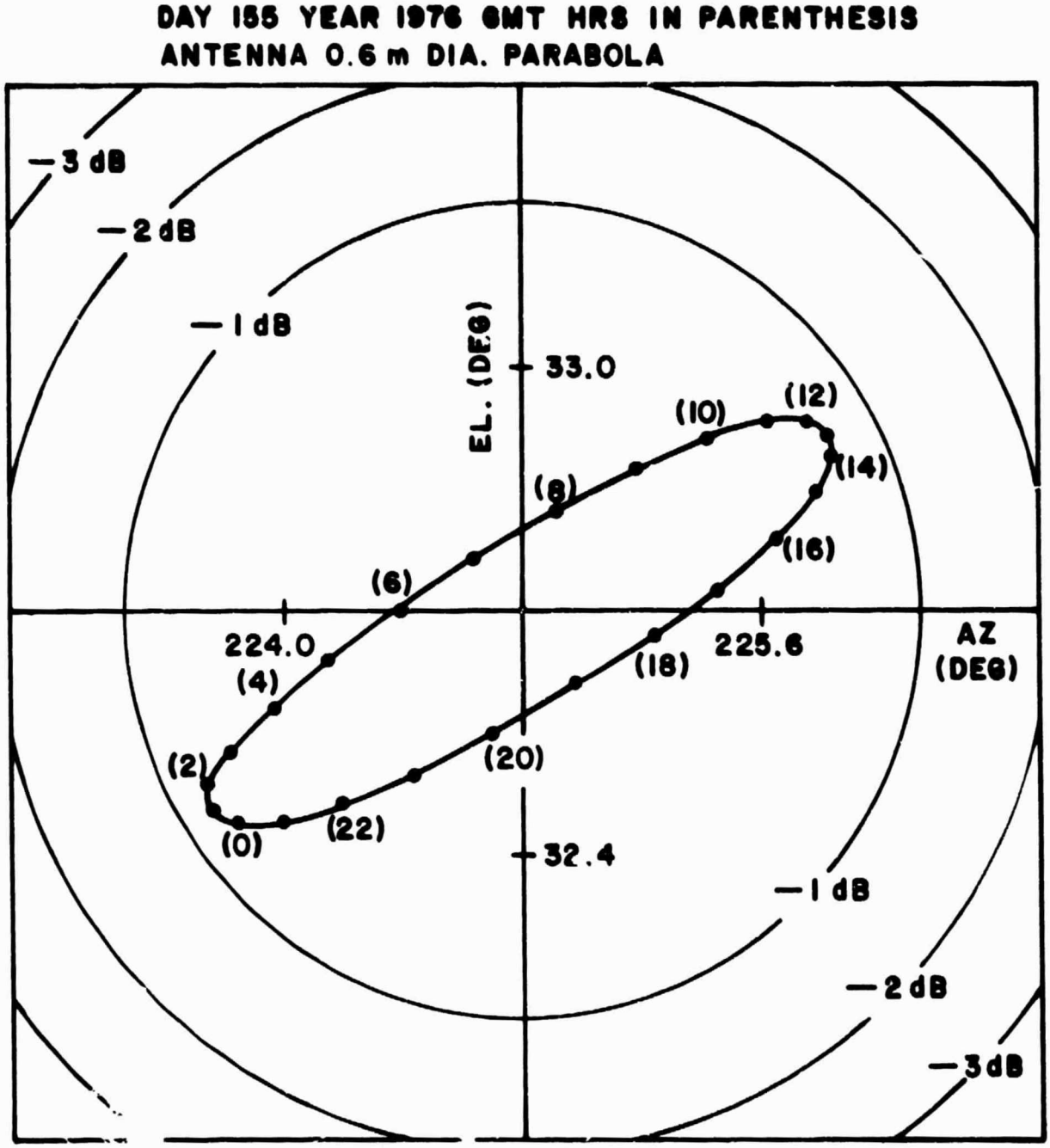

Figure 5. Diurnal motion of the spacecraft in the AZ-EL plane superimposed on the pattern contours for a single array element

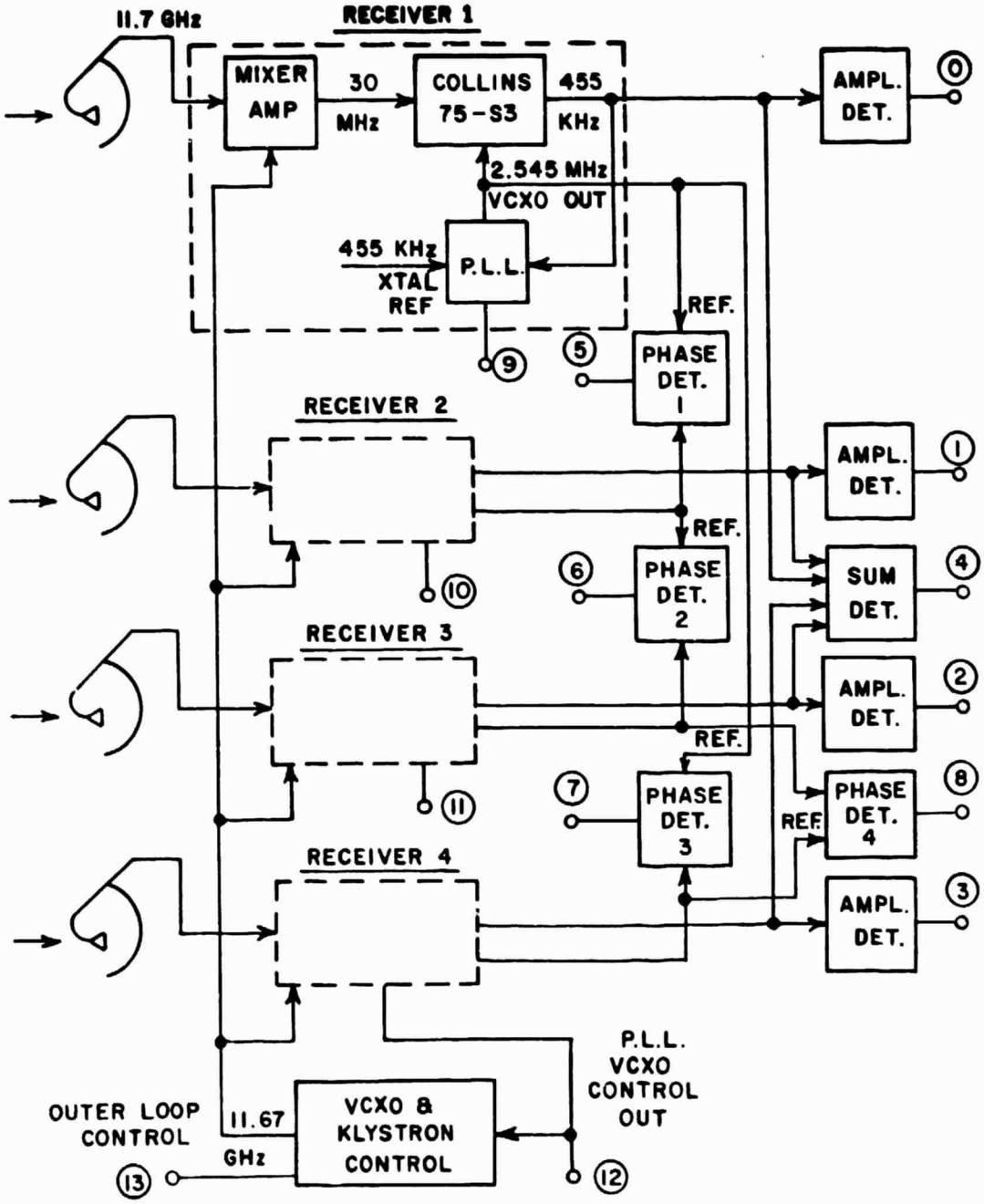

Figure 6. Self phased array receiver block diagram (the circled numbers indicate sampled and recorded variables

signal common to all array elements. This is accomplished by means of a double PLL system. The outer loop, referenced to channel 4, removes the slow, long term phase variations due to Doppler shift resulting from the diurnal motion of the spacecraft and any other sources of long term drift. The four inner loops then respond to the more rapid phase variations experienced by each channel. The four channel signals are also coherently summed to provide the array output.

Phase lock loops provide this phase alignment for the elements and stabilize the 2.545 MHz VCXO mixer injection. These VCXO outputs are also used to derive the phase differences between pairs of array elements. These differential phase measurements are used to determine the apparent angle of arrival of the incoming signal. The 2.545 MHz outputs are compared using phase detectors which are referenced as shown in Figure 6. The unambiguous output range of the phase detectors is $\pm 90^{0}$.

Amplitude detection is performed using the 455 KHz IF signal for each array element and the coherent sum. The bandwidth at 455 KHz is approximately 80 Hz. The system margin is approximately 18 dB; down link margin calculations are presented in Table 3.

Two calibration schemes are adopted in this experiment: one for the amplitudes and the other for the differential phases. These schemes are described in the following sections.

Amplitude calibration scheme

The amplitude of each PLL receiver is calibrated by injecting a 30 MHz signal and the noise from the front end at its input. Figure 7 shows that a step attenuator is used to vary the injected signal so that it ranges from the nominal clear sky level down to the receiver threshold. The average calibration curve for the four receivers is shown in Figure 8. This single curve is used for all four receivers.

Phase calibration scheme

This scheme is similar to the amplitude calibration scheme described above. Each phase detector is calibrated by means of a 30 MHz signal

TABLE 3

DOWNLINK MARGIN CALCULATIONS
11.7 GHz CTS Beacon
The OSU Satellite Communications Facility

Spacecraft:			
	Transmitter power		23.0 dBm
	System loss	-	1.0 dB
	Antenna gain		18.0 dB
Path:			
	Free space loss	-	204.9 dB
	Atmospheric gas loss	-	0.1 dB
Ground Terminal:			
	Antenna gain	+	34.7 dB
	System loss	-	0.2 dB
Received Signal:		-	130.5 dBm
	Noise figure = 7.1 dB*		
Noise Input:		-	148.7 dBm
System Margin (S/N):			18.2 dB

*This is an average figure for the four receivers whose noise figures vary from 7.0 to 7.2 dB.

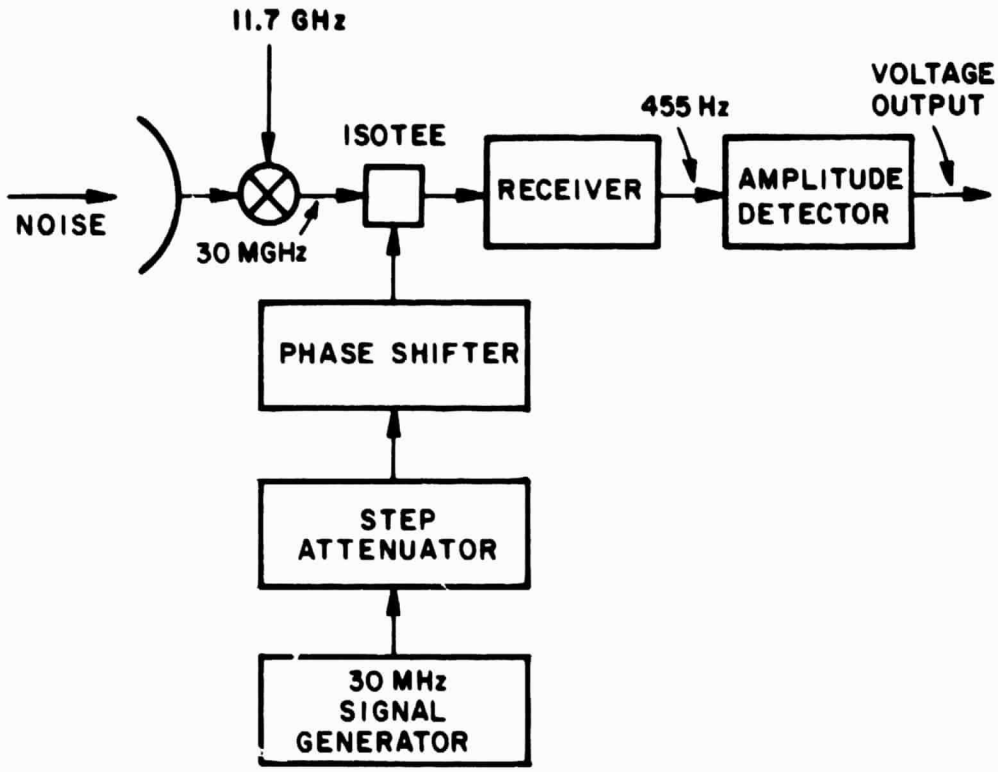

Figure 7. Test configuration for amplitude and phase calibration

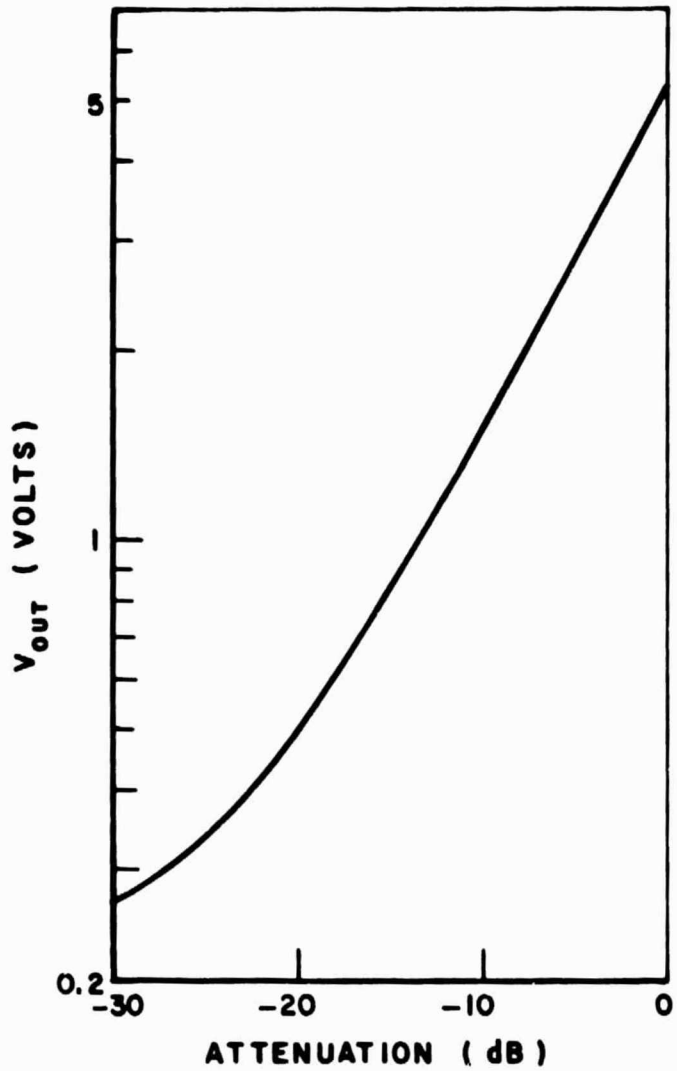

Figure 8. Average amplitude calibration curve for the four PLL receivers at 11.7 GHz

plus front end noise injected at its input. A variable phase shifter is used to change the phase of the injected signal so that the phase detector output varies from -5 to 5 volts. An average phase calibration curve is then constructed for use by all four receivers. A typical curve is shown in Figure 9.

3. The Digital System

The data acquisition process of the CTS Experiment is normally operated in a time continuous mode. However, the process can be interrupted and halted at any time. Figure 10 shows the configuration of the digital data system which handles the data acquisition process. The amplitude and phase detector outputs are multiplexed, A/D converted, buffered, and recorded on 7-track magnetic tape. The tape record format consists of a header followed by sampled data (Figure 11). Tables 4 through 8 describe the contents of the header and specify the data sampled. This acquisition process is controlled by sense switches in the digital interface. The magnetic tape unit is a 7-track Ampex unit. Digital time signals are generated by the clock interface. The serial link is utilized when the 7-track tapes are copied onto the 9-track tapes, which are analyzed by programs running on the Datacraft 6024 computer in the ElectroScience Laboratory. The HP 2116B computer coordinates the above components in the digital system.

It should be noted that there are two sampling rates adopted in this experiment. The data are normally recorded at a rate of 1/3 Hz and can be switched to 10 Hz on demand. This report uses only the data sampled at 1/3 Hz. Economic use of tapes is the primary reason for using the slower sampling rate. It is realized that the Nyquist sampling rate criterion does not play a role here since only the temporal mean and variance of signal attenuation and angle scintillation are generated.

III. DATA ANALYSIS

Table 9 lists the data periods in 1976-1978, during which measurements were made. The total data time recorded on magnetic tape for

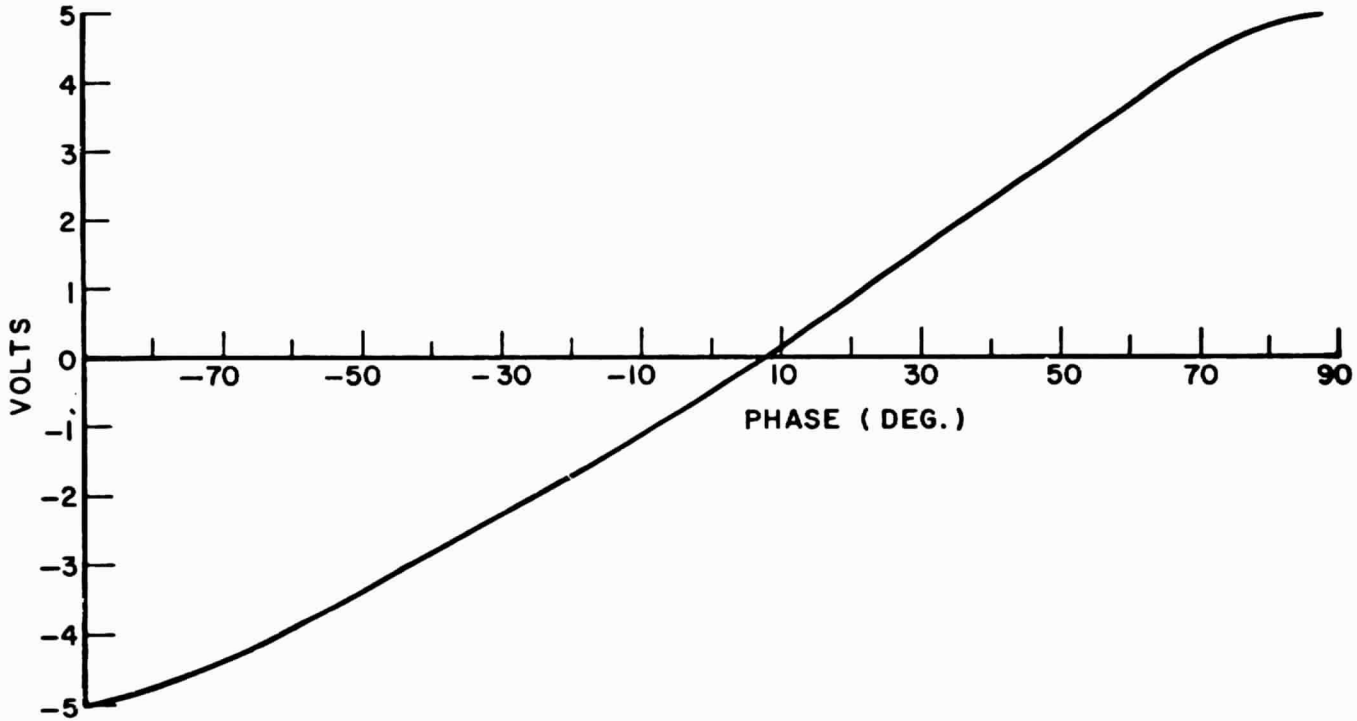

Figure 9. Phase calibration curve.

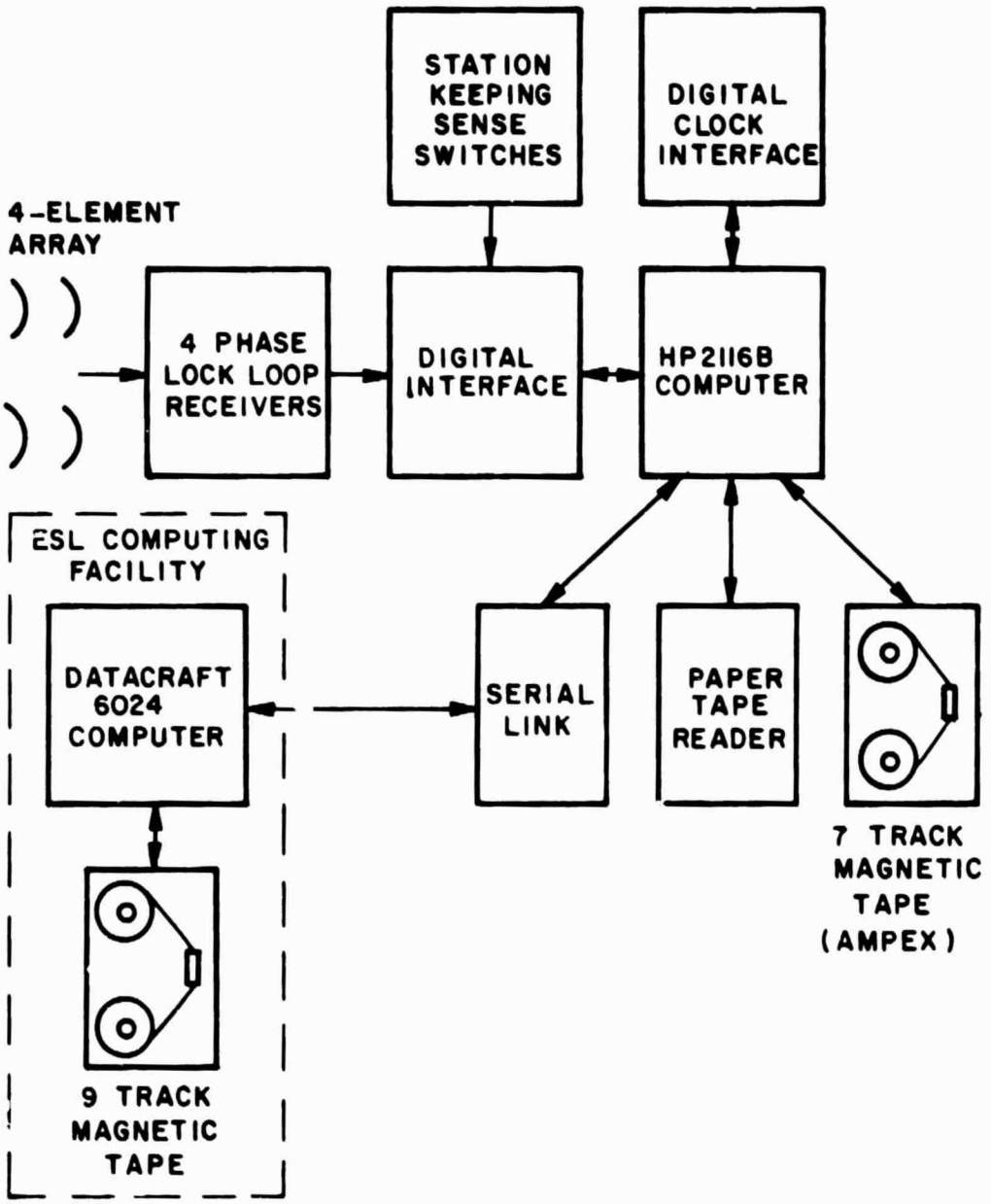

Figure 10. The digital data system configuration.

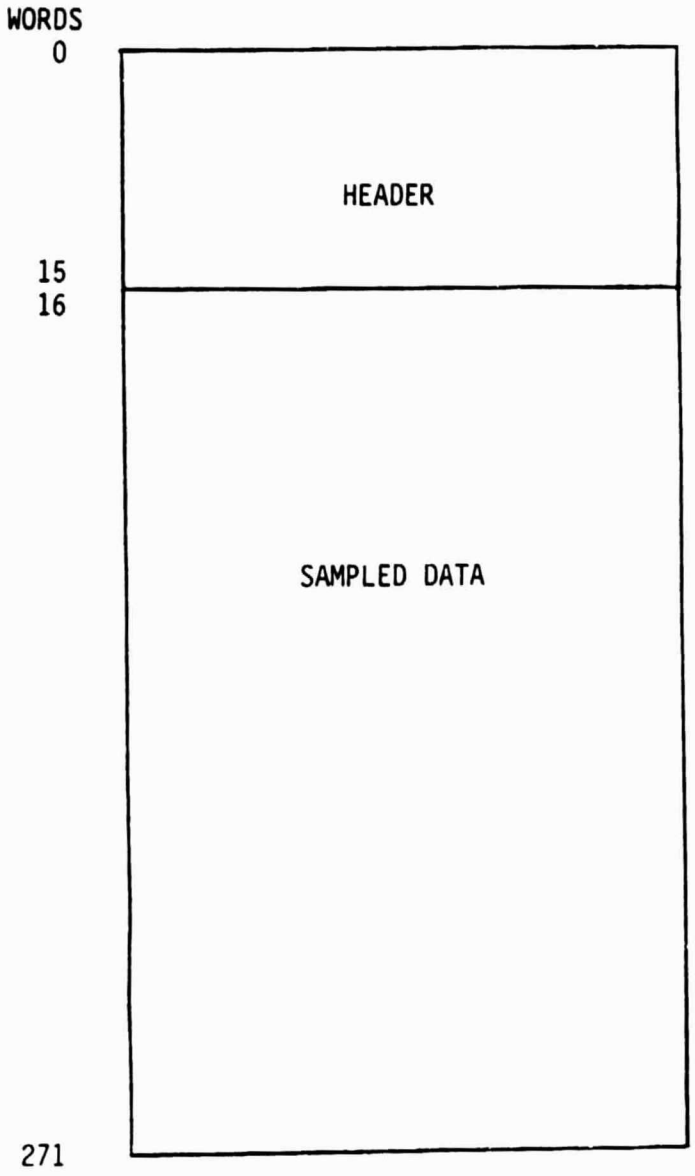

Figure 11. Tape record format.

TABLE 4

TAPE RECORD HEADER FORMAT

WORD NO.	CONTENTS
0	No. of words in record
1	Record type
2	Status word 1
3	Status word 2
4	Status word 3
5	Millisecond count
6	Clock word 1
7	Clock word 2
8	Clock word 3
9	Fast queue interval
10	Slow queue interval
11	No. of samples in record
12	Spare
13	Spare
14	Spare
15	Spare

TABLE 5

STATUS WORDS - CTS

BIT NO.	WORD 1	WORD 2	WORD 3
0	Slow only	Cal. AØ	1
1	Fast only	Cal. A1	2
2	Slow and fast	Cal. A2	4
3	Unassigned	Cal. A3	8
4	Unassigned	Cal. A4	16
5	Unassigned	Cal. A5	32
6	Unassigned	Cal. A6	64
7	Unassigned	Cal. A7	128
8	Unassigned	Cal. BØ	256
9	Unassigned	Cal. B1	512
10	Radiom. with calibration	Cal. B2	Unassigned
11	Radiom. only	Cal. B3	Unassigned
12	Unassigned	Cal. B4	Unassigned
13	Unassigned	Cal. B5	Unassigned
14	Idle	Cal. B6	Unassigned
15	Stop	Cal. B7	Unassigned

Modulo 1000 Computer

TABLE 6

REAL-TIME-CLOCK WORDS

BIT NO.	CLOCK WORD 1	CLOCK WORD 2	CLOCK WORD 3
0	1 ⎫	1 ⎫	1 ⎫
1	2 ⎬ Seconds, units	2 ⎬ Minutes, tens	2 ⎬ Days, units
2	4 ⎭	4 ⎭	4
3	8	1 ⎫	8 ⎭
4	1 ⎫	2	1 ⎫
5	2 ⎬ Seconds, tens	4 ⎬ Hours, units	2 ⎬ Days, tens
6	4 ⎭	8 ⎭	4
7	1 ⎫	1 ⎫	8 ⎭
8	2 ⎬ Minutes, units	2 ⎭ Hours, tens	1 ⎫ Days, hundreds
9	4	Unassigned	2 ⎭
10	8 ⎭	Unassigned	Unassigned
11	Unassigned	Unassigned	Unassigned
12	Unassigned	Unassigned	Unassigned
13	Unassigned	Unassigned	Unassigned
14	Unassigned	Unassigned	Unassigned
15	Unassigned	Unassigned	Unassigned

TABLE 7

RECORD TYPE 12, 13 FORMAT
(Fixed Terminal - CTS)

	0 : 15	Header														
		15	14	13	12	11	10	9	8	7	6	5	4	3	2	1	0
Sample 1	16	Channel 0								Channel 1							
	17	Channel 2								Channel 3							
	18	Channel 4								Channel 5							
	19	Channel 6								Channel 7							
	20	Channel 8								Channel 9							
	21	Channel 10								Channel 11							
	22	Channel 12								Channel 13							
		Channel 14								Channel 15							
Sample 2 : Sample N																	

Type 13 (Slow) — [N_{max} = 32 (272 word record) Corresponding to 96 seconds]

Type 12 (Fast) — [N_{max} = 32 (272 word record) Corresponding to 3.2 seconds]

TABLE 8

FIXED TERMINAL CHANNEL ASSIGNMENTS - CTS

CHANNEL	SOURCE	REC TYPE	DATA RATE (Samp./sec)	FILTER (f_{3dB})
0	R_1 Amp	13, 12	1/3, 10	10
1	R_2 Amp	13, 12	1/3, 10	10
2	R_3 Amp	13, 12	1/3, 10	10
3	R_4 Amp	13, 12	1/3, 10	10
4	Σ Amp	13, 12	1/3, 10	10
5	$\emptyset_1$	13, 12	1/3, 10	10
6	$\emptyset_2$	13, 12	1/3, 10	10
7	$\emptyset_3$	13, 12	1/3, 10	10
8	$\emptyset_4$	13, 12	1/3, 10	10
9	$VCXO_1$	13, 12	1/3, 10	10
10	$VCXO_2$	13, 12	1/3, 10	10
11	$VCXO_3$	13, 12	1/3, 10	10
12	$VCXO_4$	13, 12	1/3, 10	10
13	Spare	13, 12	1/3, 10	10
14	Spare	13, 12	1/3, 10	10
15	Spare	13, 12	1/3, 10	10

TABLE 9

SUMMARY OF CTS ANGLE OF ARRIVAL DATA PERIODS

MONTH	HOURS OF DATA
May, 1976	373
June	554
July	223[1]
August	474[2]
September	---[2]
October	---[2]
November	---[3]
December	416
January, 1977	526[4]
February	481
March	423
April	570
May	514
June	648
July	417
August	249[5]
September	403
October	500
November	625
December	572
January, 1978	626
February	270[6]
March	487
April	552
May	657
TOTAL	10,559

[1]Data system tape failure and system modification
[2]ATS-6 return period 8/27/76 to 10/16/76
[3]Receiver failure
[4]Commencement of large frequency excursions
[5]Air conditioner failure
[6]Coal shortage

the duration of the experiment is approximately 10,599 hours. After processing, the total data base is 6356 hours. Data were discarded during the data editing process for the following reasons: (1) more than one receiver was not phase locked; (2) the integrity of data is questionable; or (3) short records (records with less than thirty-two samples) occurred when a sense switch was altered or in the event of a power failure.

In January, 1977, the beacon signal began to exhibit erratic frequency excursions. These erratic excursions ranged from small abrupt jumps up to several Kilohertz over periods of a few hours. The existence of these excursions and their magnitudes were confirmed by measurements at the Communications Research Centre, Ottawa, Canada. Unfortunately, these excursions significantly degraded the quality of the phase data obtained during the course of this experiment. A sample plot of the frequency excursions on Days 41 and 42, 1977, is shown in Figure 12.

The editing process is normally done through the use of an interactive CRT display and light pen. Extensive computer programs have been developed for the analysis of these data in the ElectroScience Laboratory Datacraft 6024 computer. Monthly and annual cumulative distribution curves of signal amplitudes and differential phases are generated. Rain fades are plotted and analyzed. A typical rain fade analysis is presented later in this report.

For each record of data (i.e. thirty-two samples over 96 seconds), the mean signal amplitude, amplitude variance, mean differential phase angle, and phase variance are calculated. These statistical quantities are defined as follows:

(i) mean amplitude

$$\overline{V} = \frac{1}{N} \sum_{i=1}^{N} V_i \qquad [\text{volts}] \qquad N = 32 \qquad (4)$$

where V_i is the sampled value of the amplitude detector output voltage v(t).

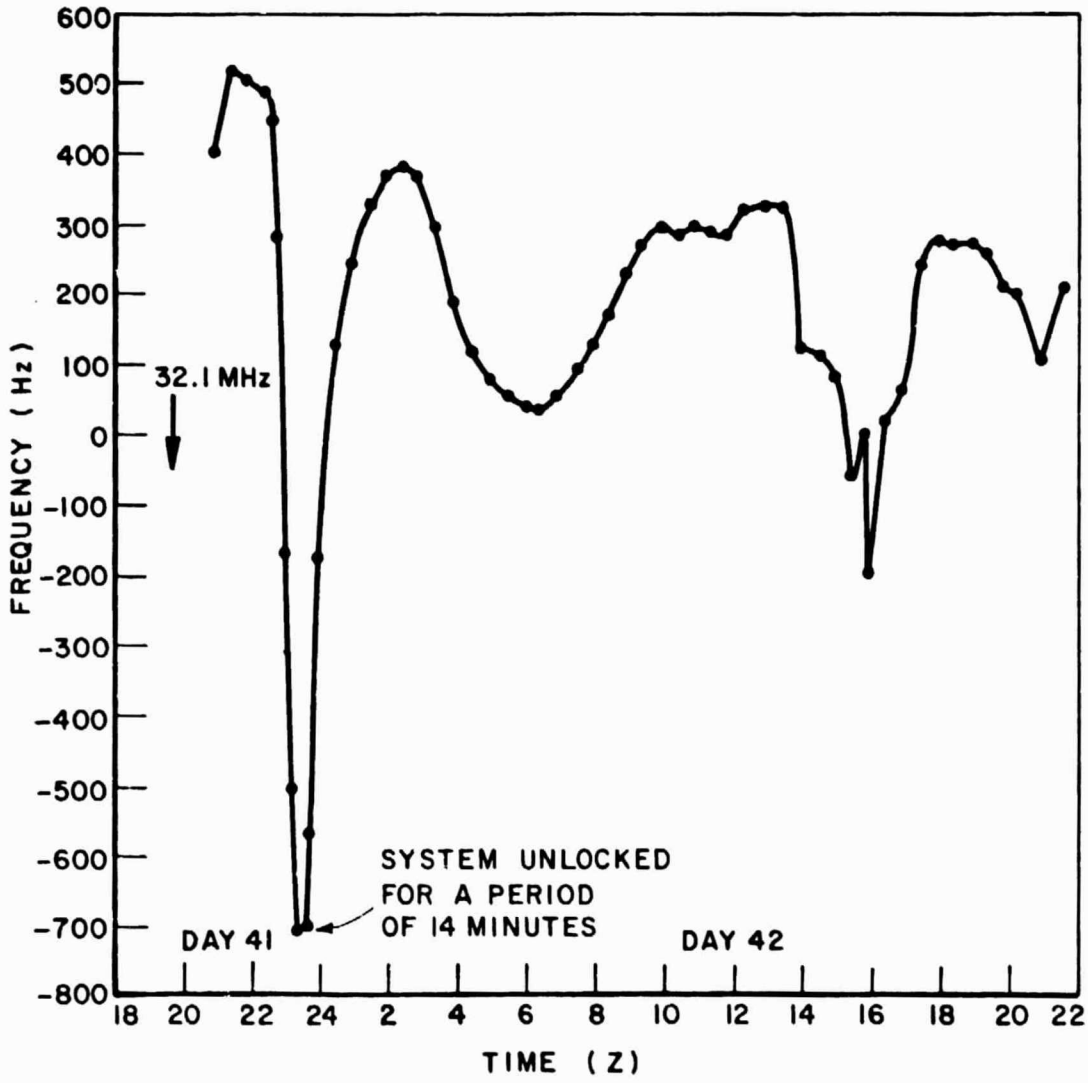

Figure 12. Beacon frequency: days 41 and 42, 1977.

(ii) amplitude variance normalized with respect to the DC power level for N samples

$$\sigma_A^2 = 10 \log_{10} \left[\frac{\sum_{i=1}^{N} (V_i - \bar{V})^2}{N\bar{V}^2} \right] \qquad [\text{dB}] \quad N = 32 \qquad (5)$$

(iii) mean phase

$$\bar{\Phi} = \frac{1}{N} \sum_{i=1}^{N} \Phi_i \qquad [\text{degree}] \quad N = 32 \qquad (6)$$

where $_i$ is the sampled value of the differential phase $\Phi(t)$ between two received signals.

(iv) phase variance

$$\sigma_\Phi^2 = 10 \log_{10} \left[\frac{\sum_{i=1}^{N} (\Phi_i - \bar{\Phi})^2}{N\Phi_o^2} \right] \qquad [\text{dB}] \quad N = 32 \qquad (7)$$

where Φ_o is an arbitrary constant which is chosen such that σ_Φ^2 is normalized to 1 degree squared.

Projection Algorithm

During the analysis process, it is important to observe both the signal amplitude and the differential phase fluctuations about appropriate reference levels. In order to establish these reference levels, it is necessary to remove any slow, long term variations in the data such as those resulting from the diurnal motion of the spacecraft.

In the following, two reference levels are defined:

(1) Amplitude reference level (mean max)

$$m_A \triangleq \frac{1}{N} \sum_{i=1}^{N} \max_{1 \le j \le 32} V_{ij} \qquad \text{dB} \qquad (8a)$$

(2) Differential phase reference level (mean)

$$m_{\phi} = \frac{1}{N} \sum_{i=1}^{N} \left(\frac{1}{32} \sum_{j=1}^{32} \phi_{ij} \right) \quad \text{dB} \qquad (8b)$$

where V_{ij} and ϕ_{ij} are the calibrated sampled values in record i which contains thirty-two sampled values. N is the number of records in each data segment being analyzed. It should be noted that forty records correspond to about 60 minutes of data. In the projection algorithm described below,

$$N = \begin{cases} 13 & \text{for the four initial data segments} \\ 40 & \text{after the four initial data segments} \end{cases}$$

Since the data acquisition process is subject to interruptions, the data set consists of data segments of various numbers of records. The flow chart in Figure 13 shows the algorithm employed in computing and projecting the reference levels. This algorithm performs an appropriate polynomial fit to the amplitude and phase reference levels so that these levels can be projected forward in time. In this manner, the reference levels can be established and maintained through periods of rain fading or other signal disturbances.

It should be noted that in projecting the amplitude mean level, the projected mean is ignored if it is more than 5 dB below the most recent mean level. In this manner, an amplitude reference level can be established so that attenuation can be measured during fade events. This criterion does not apply to the projection of the differential phase mean level.

IV. RESULTS

In this section, the results of the data analysis are discussed and the statistics of the CTS measurements are presented. Two examples of typical rain events are shown in Figures 14 and 15. In each case, the upper trace shows the received signal (array sum amplitude) and the lower two traces show the differential phases for azimuth and elevation element pairs, respectively. The curves shown are max-min

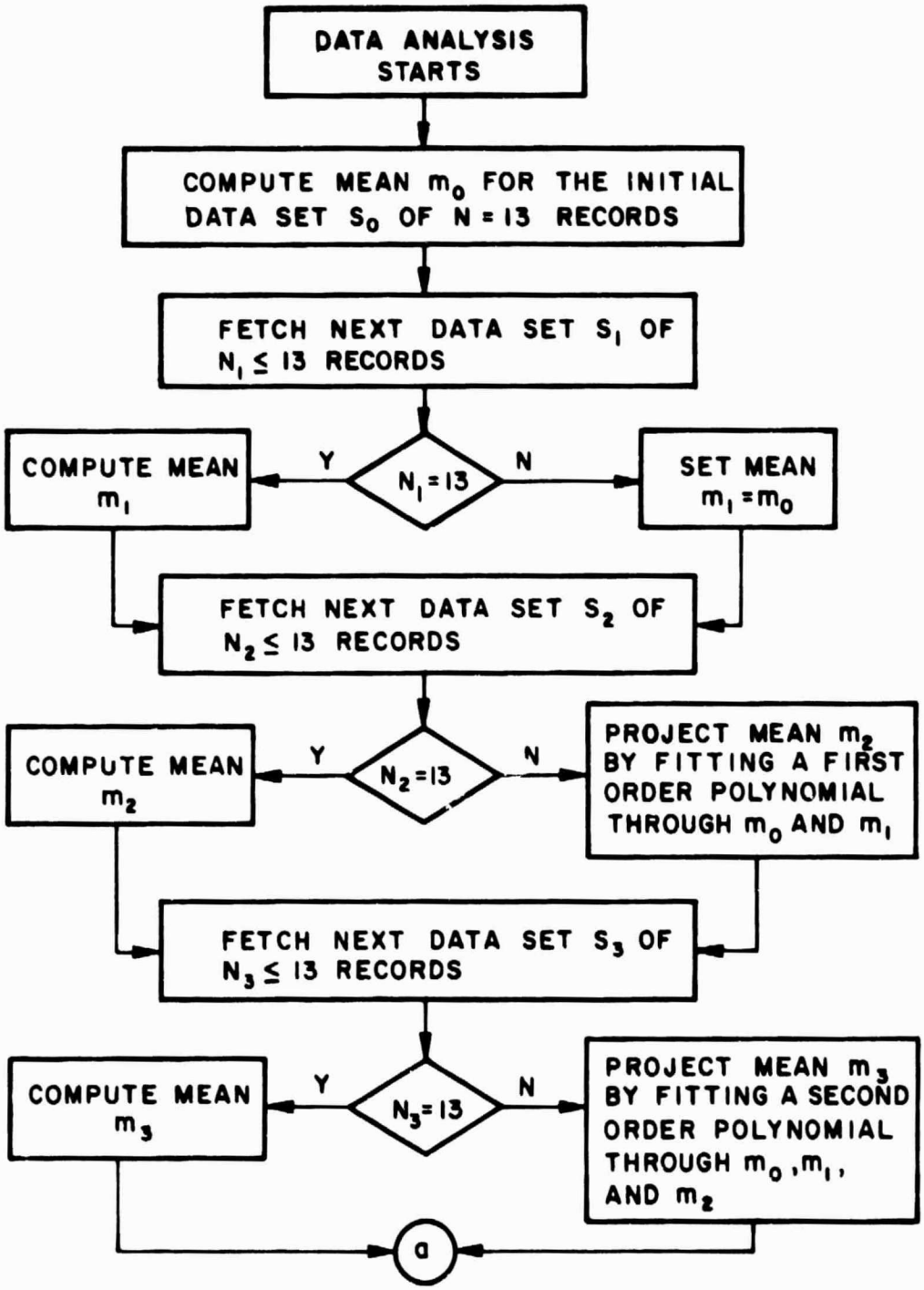

Figure 13. Flow chart for computing and projecting reference mean levels.

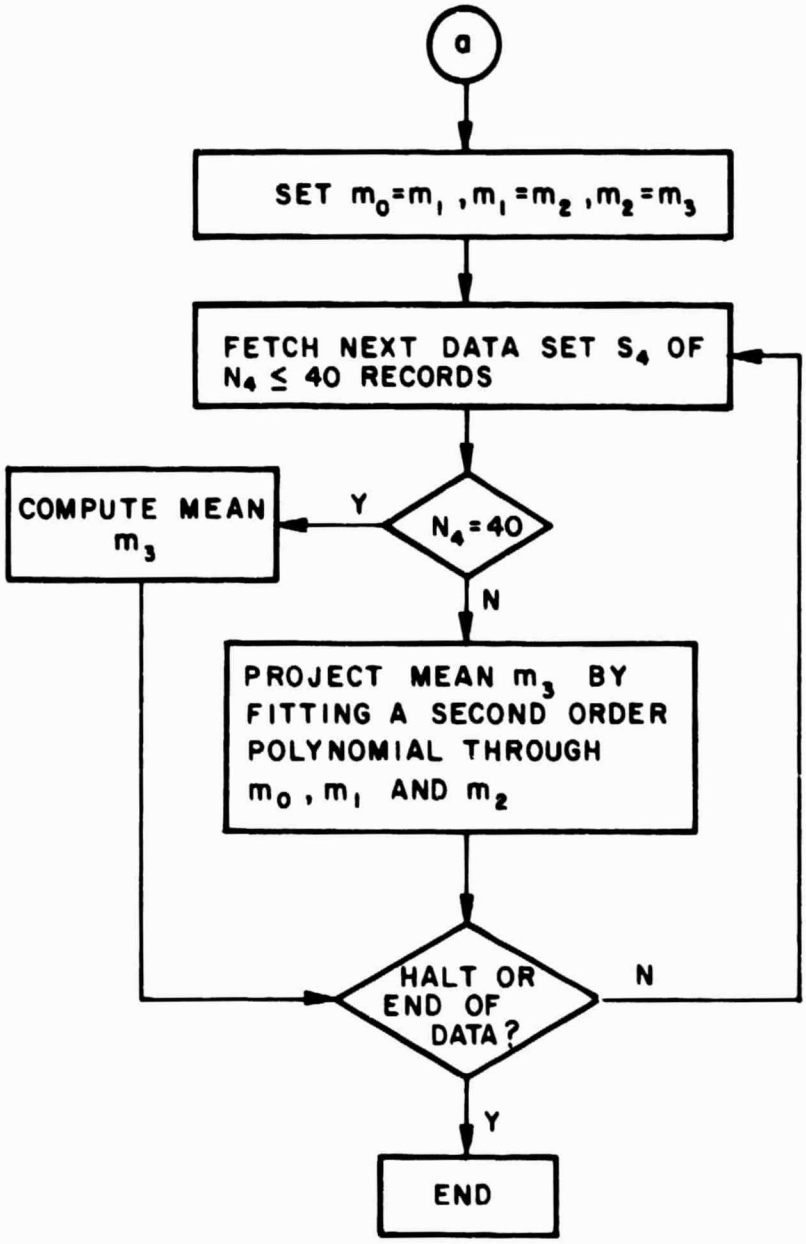

Figure 13 (continued)

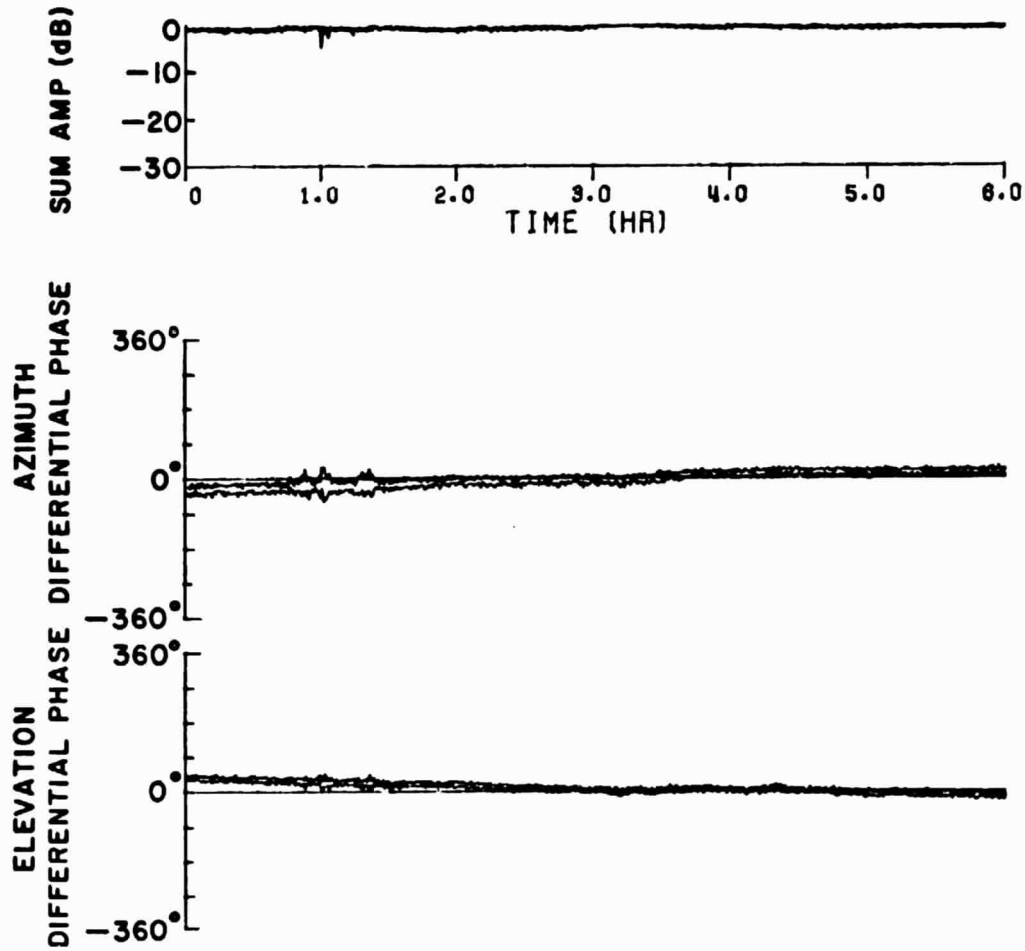

Figure 14. CTS 11.7 GHz beacon: day 73 13H 18M 47S (1977).

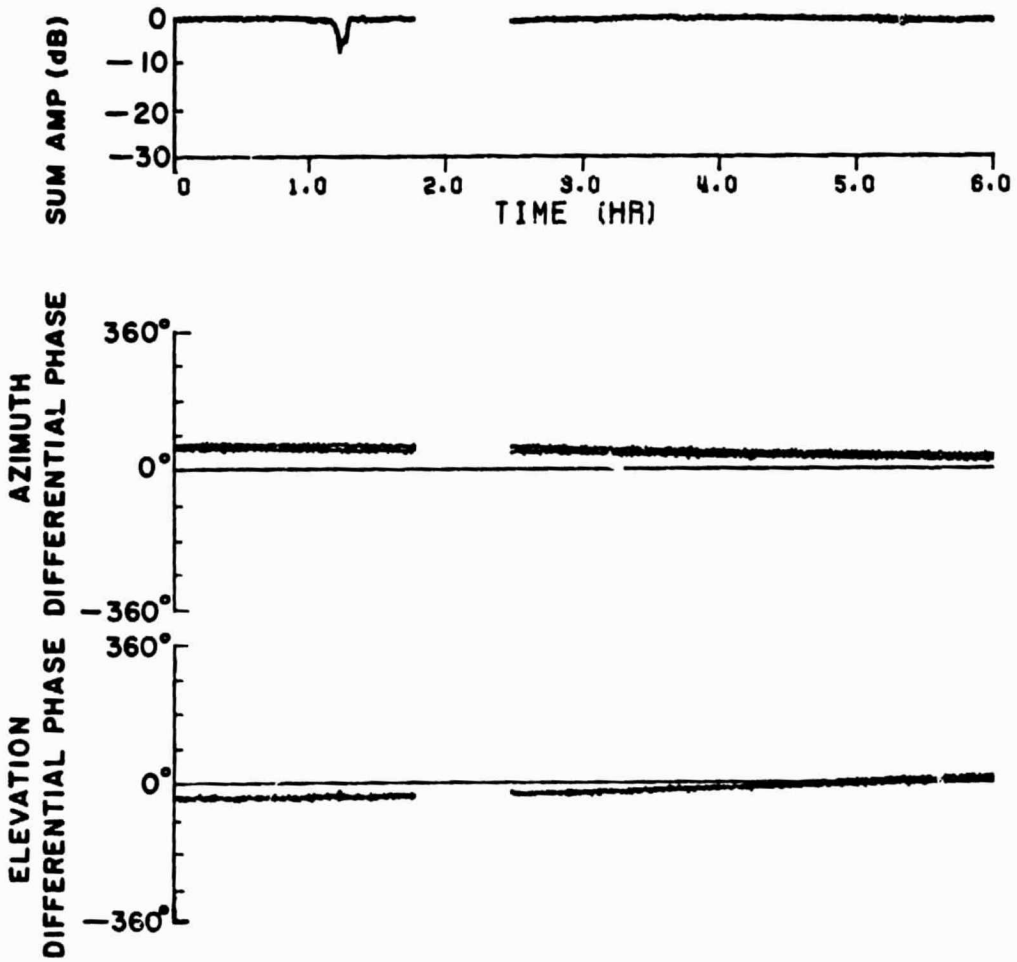

Figure 15. CTS 11.7 GHz beacon: day 94 18H 43M 3S (1977).

envelopes where the maximum and minimum values for each 96-second period are plotted.

In Figure 14, a small, 4-dB fade occurred near the one-hour time mark. Prior to, during, and after this fade, the elevation differential phase fluctuated as much as 90^{o}; this fluctuation corresponds to an apparent angle of arrival change larger than 0.3^{o}. In Figure 15, a larger, 8-dB fade was observed with no significant increase in the differential phases. This pair of cases should clearly show that the observed differential phase fluctuations are not due to decreases in the signal-to-noise ratio during fade events.

A sample of the signal received on Day 193, 1977, is presented in Figure 16. This thirty-minute data period contains a 15-dB rain fade. Samples obtained every three seconds are plotted with no integration. The upper curve shows the array sum amplitude, while the lower traces show the electrical phase differences between a pair of array elements in the azimuth plane and a pair of array elements in the elevation plane. It should be noted that the peak-to-peak phase fluctuations prior to and after the fade are on the order of 40^{o}. However, during the fade this value increases to approximately 140^{o}. Therefore, it is clear that the outputs of the individual elements cannot be summed effectively to produce the full array gain unless some form of adaptive phase compensation is employed.

Figure 17 shows another 7-dB rain fade event lasting approximately five minutes on Day 233, 1977. The sum amplitude data for this case have been averaged over twenty samples, i.e. sixty seconds, and replotted in Figure 18. Also shown in Figure 18 are the averaged samples for the amplitude output from a single array element. Both of these data sets have been adjusted to an average reference level of 0 dB over the non-fading period from fifteen to twenty-five minutes. It is noted that the sum amplitude falls below, i.e. fades to a greater depth, for all values below 2 dB. The average amplitude difference during the period five to ten minutes is 0.5 dB. It should also be noted in Figure 17 that the elevation differential phase excursions are biased in the positive direction. Such a bias could result from refractive bending along the ray path.

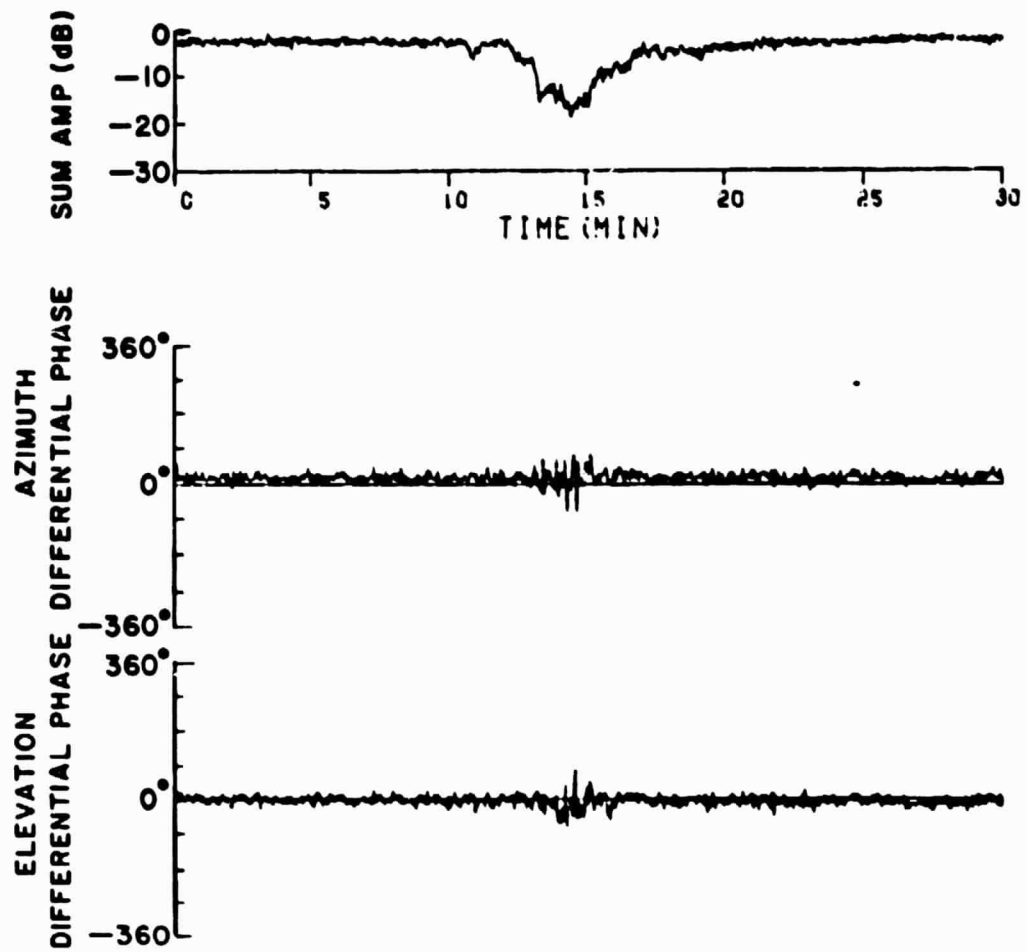

Figure 16. CTS 11.7 GHz beacon: day 193 21H 58M 58S (1977).

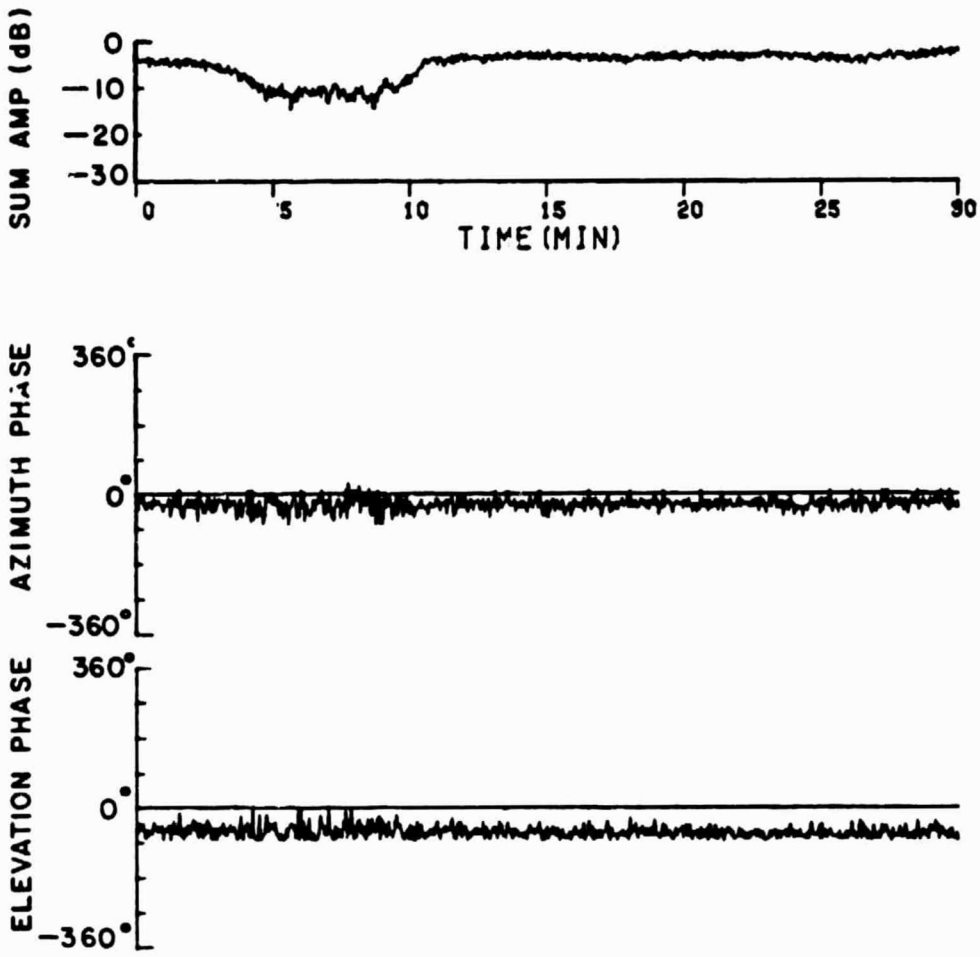

Figure 17. CTS 11.7 GHz beacon: day 233 19H 2M 25S (1977).

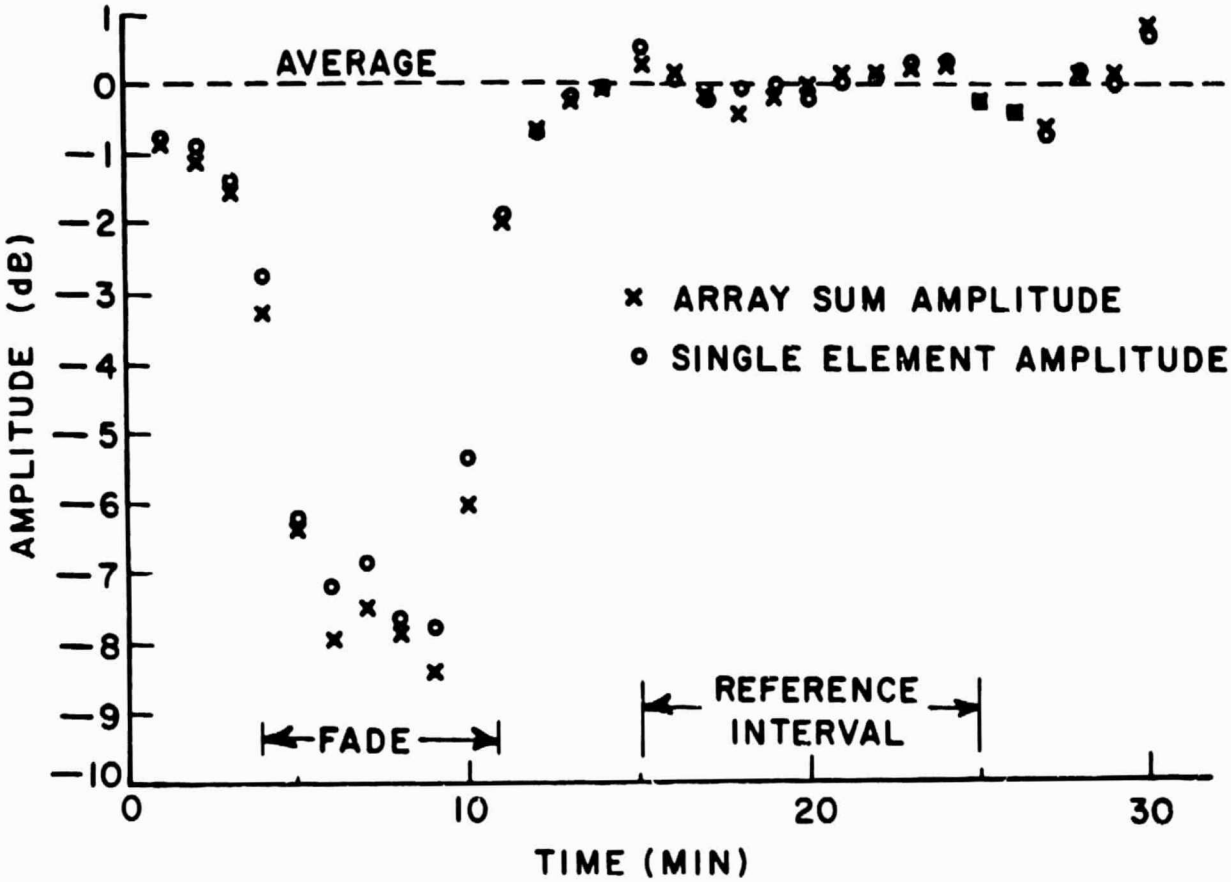

Figure 18. CTS 11.7 GHz beacon: day 233 19H 2M 25S (1977). Comparison of array and single element fading.

Clearly, the absorption experienced by both signals must be the same; therefore, the greater fading experienced by the array sum amplitude must be a result of the inability of the PLL's to compensate for the rapidly varying phase fluctuations. Since the fade is relatively shallow and does not approach the threshold of the receiving system, one must conclude that degraded signal-to-noise ratio is not the cause of this increased apparent attenuation. Thus, it seems reasonable to conclude that the array output suffers loss due to both absorption along the propagation path and the fluctuation in the apparent angle of arrival.

These two examples are typical of the results observed in general. Rain fades are usually accompanied by increased electrical phase difference fluctuations.

Attenuation Statistics

Distributions of attenuation extracted from the 11.7 GHz beacon observations are plotted in Figures 19-23. Figure 19 contains the individual distribution curves for May, June, and August, 1976, and the overall distribution for this period. Similar plots for 1977 and 1978 are shown in Figures 20, 21, and 22. The distribution curves in Figure 23 indicate that the attenuation distributions for 1976, 1977, and 1978 are surprisingly similar.

The distribution curves for the signal variance are presented in Figures 24-27. In Figure 25, it is apparent that the variance is approximately 10 dB higher during the period of January-November, 1977. It is believed that this increase is due to the erratic frequency excursions of the satellite beacon noted earlier and, thus, this particular data interval is suspect. It will be noted below that the phase statistics show this same characteristic. Ignoring this period, it can be observed that the minimum received amplitude fluctuations were 40 dB below the DC carrier power. This indicates that the receiver noise was no higher than this level. For short periods of time, i.e. during rain events in particular, the variance increased as much as 20 dB above this threshold. This increase should be tempered by the fact that the signal statistics are not stationary during fade events. Nevertheless,

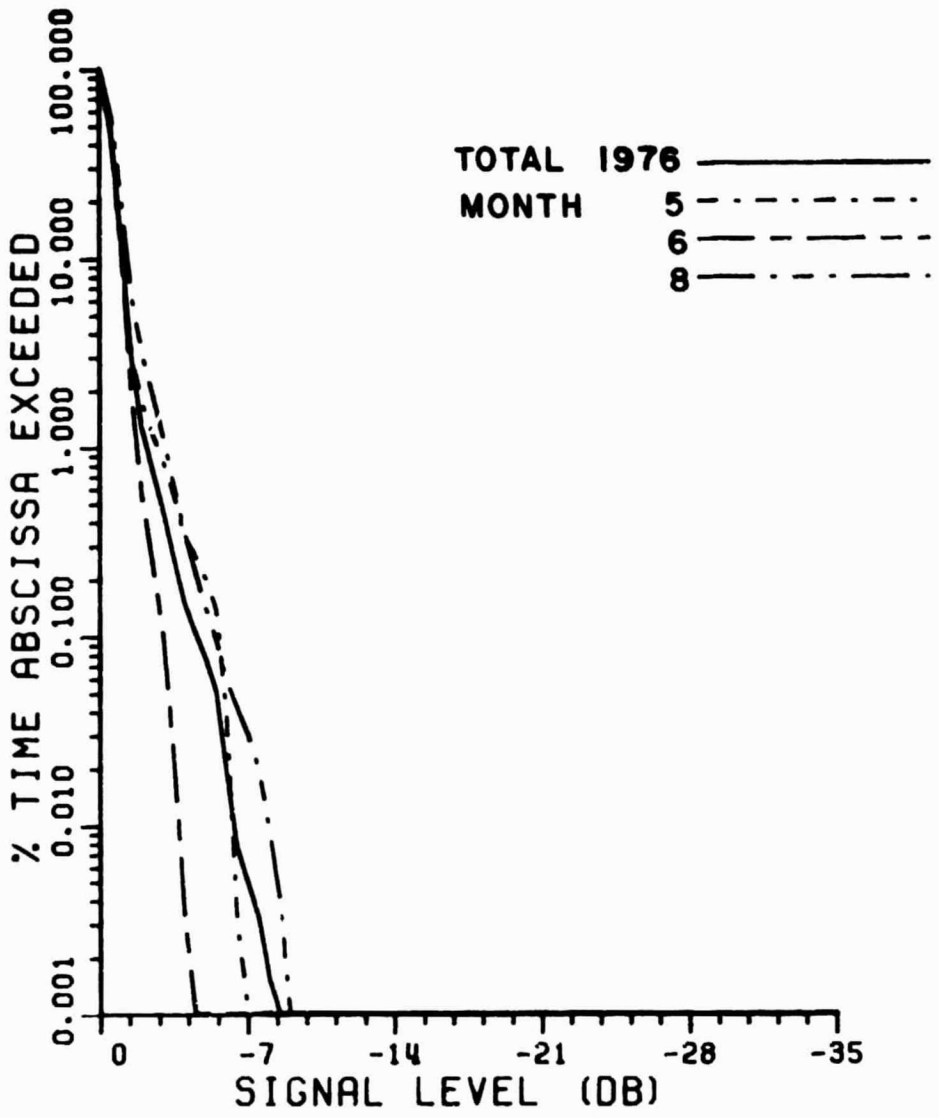

Figure 19. Cumulative distributions of sum amplitude for May, June, and August, 1976. The solid line denotes the total distribution.

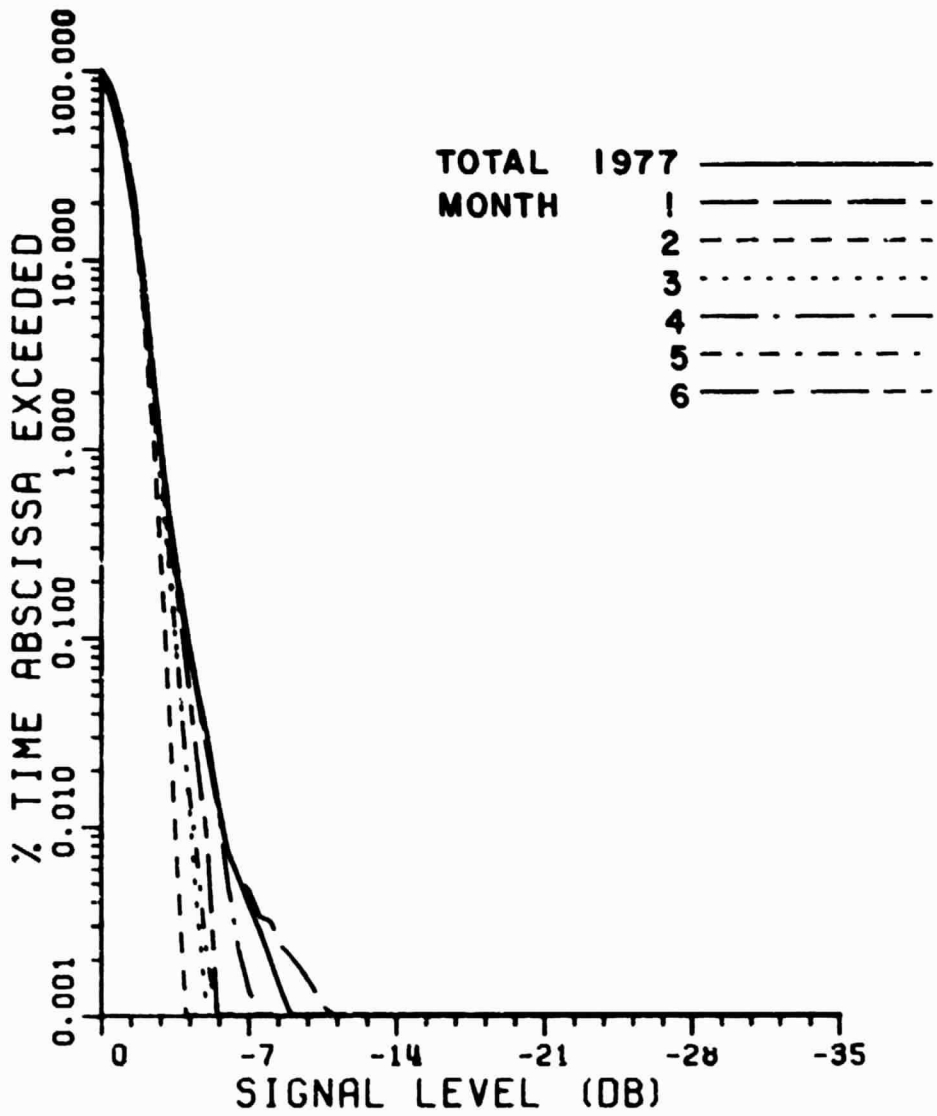

Figure 20. Cumulative distributions of sum amplitude for January-June, 1977. The solid line denotes the total distribution for 1977.

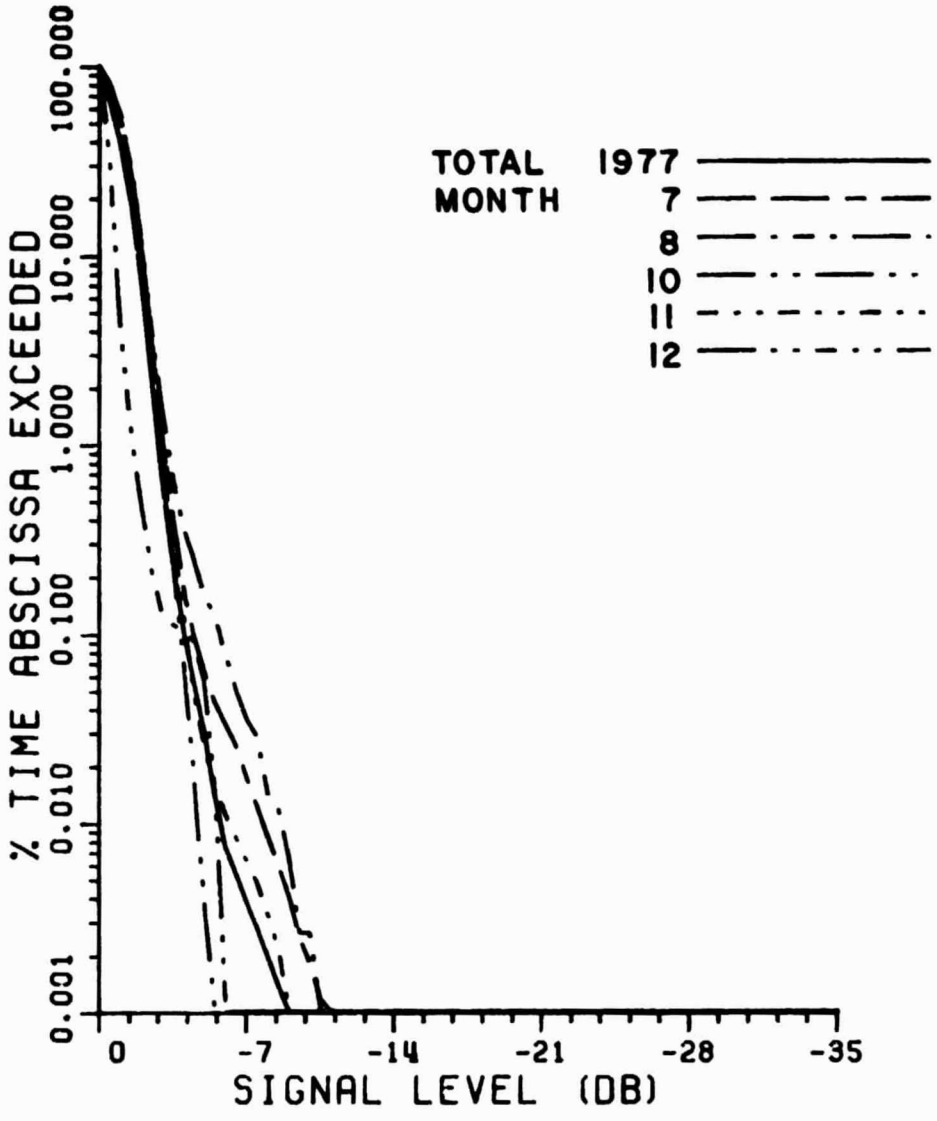

Figure 21. Cumulative distributions of sum amplitude for July-December, 1977. The solid line denotes the total distribution for 1977.

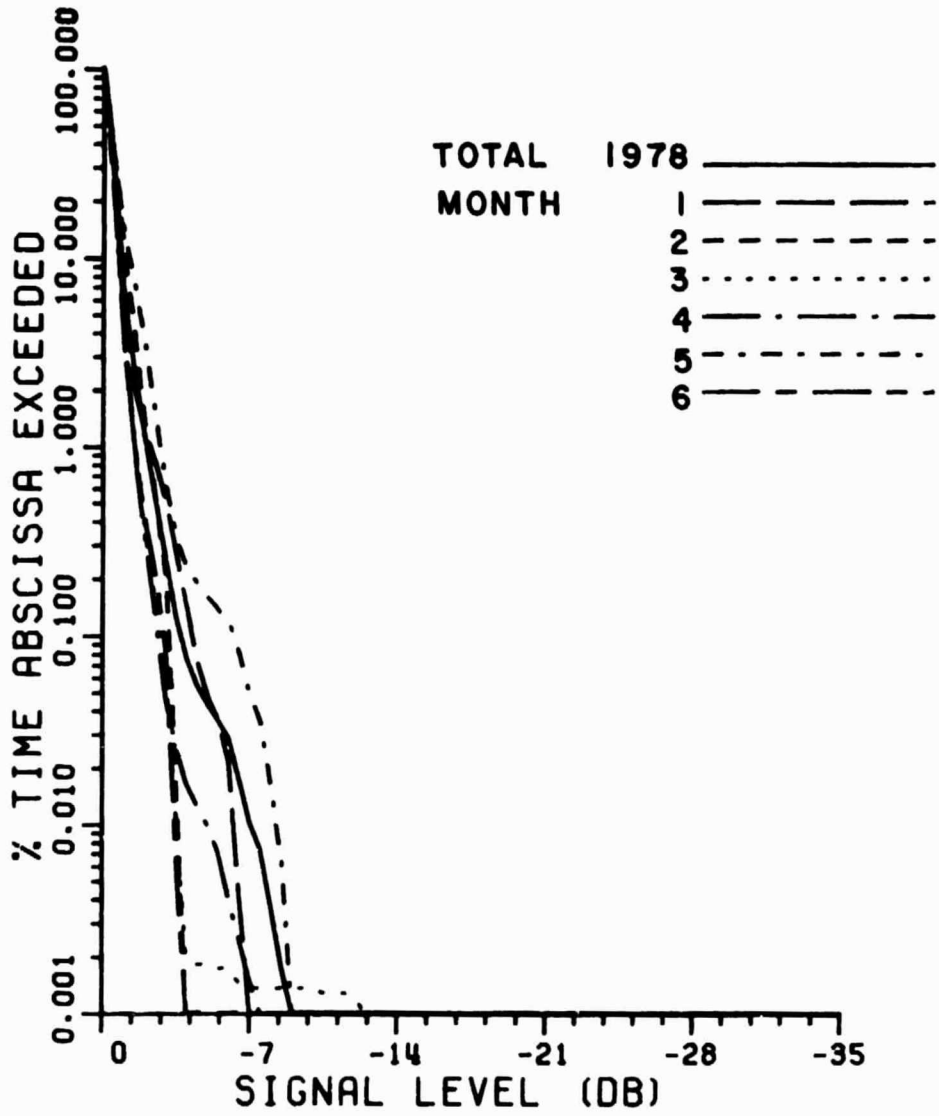

Figure 22. Cumulative distributions of sum amplitude for January-June, 1978. The solid line denotes the total distribution for 1978.

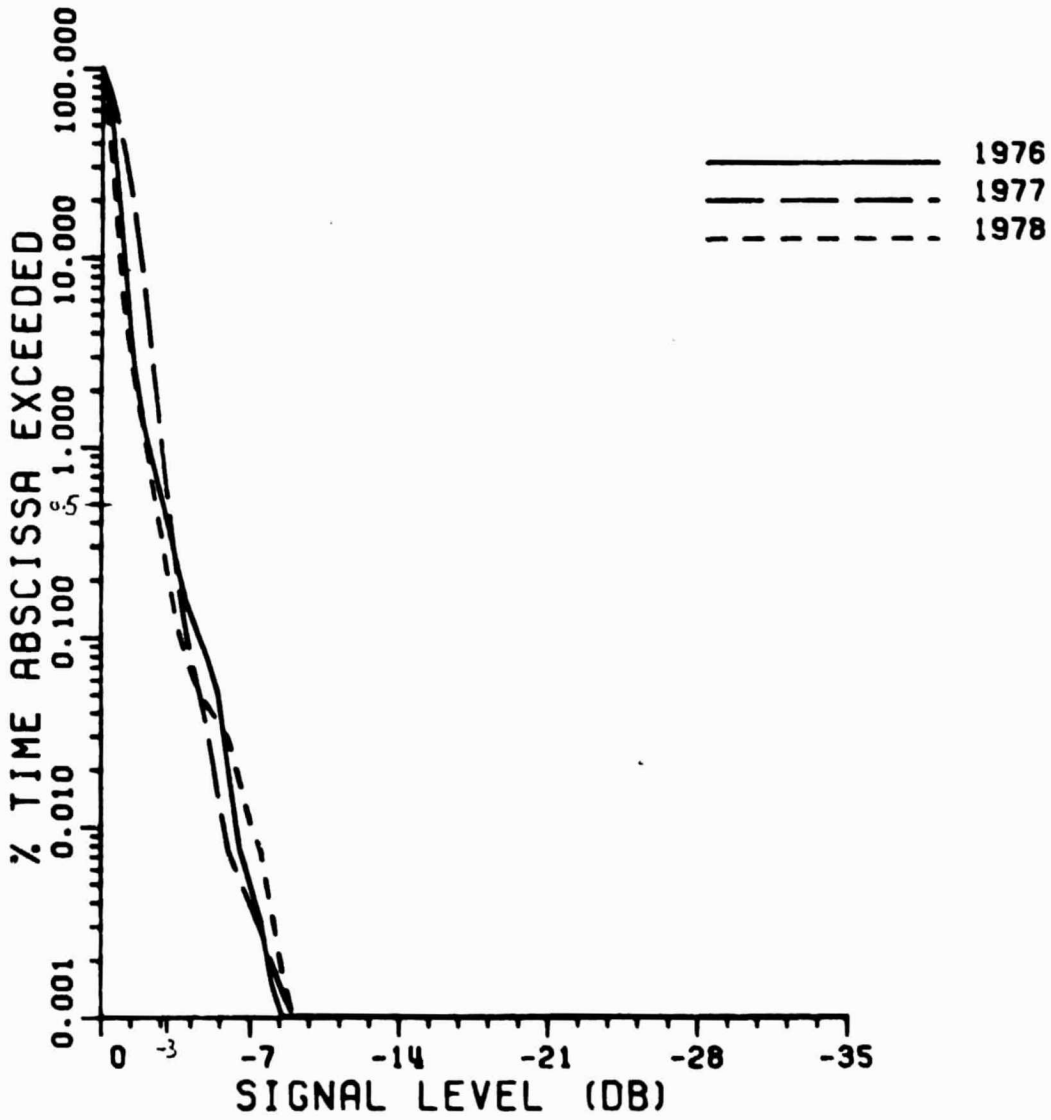

Figure 23. Cumulative distributions of sum amplitude for 1976, 1977, and 1978.

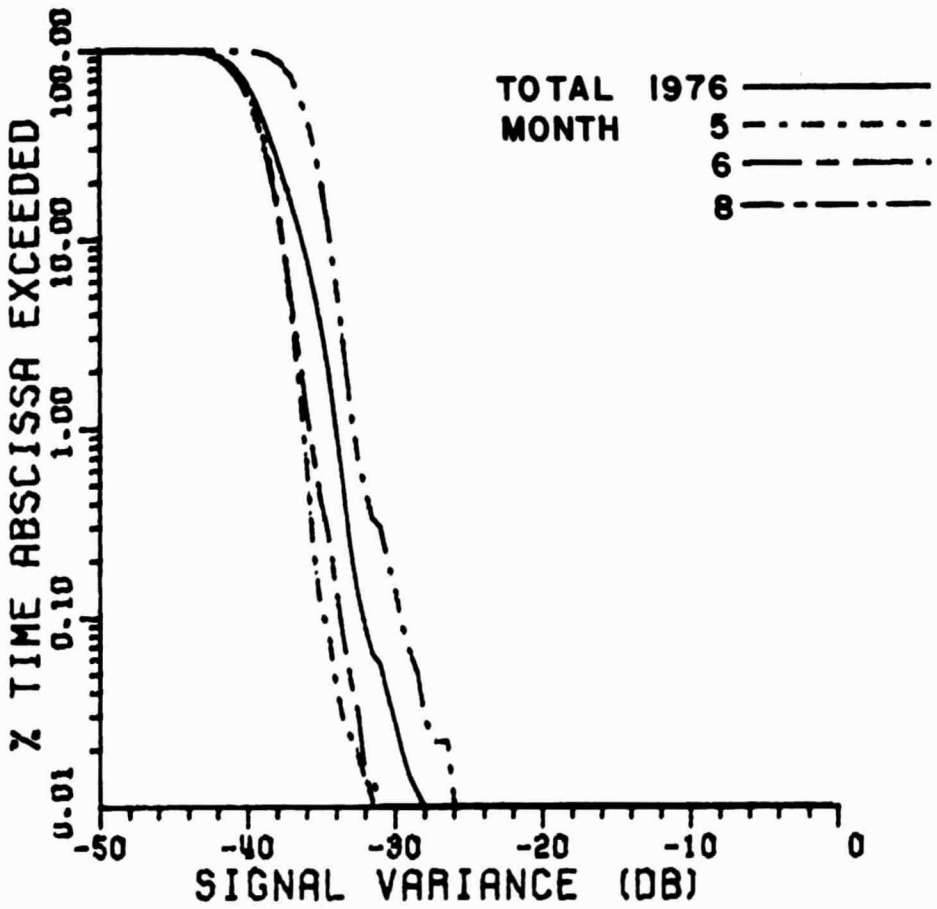

Figure 24. Cumulative distributions of sum amplitude variance for May, June, and August, 1976. The solid line denotes the total distribution for 1976.

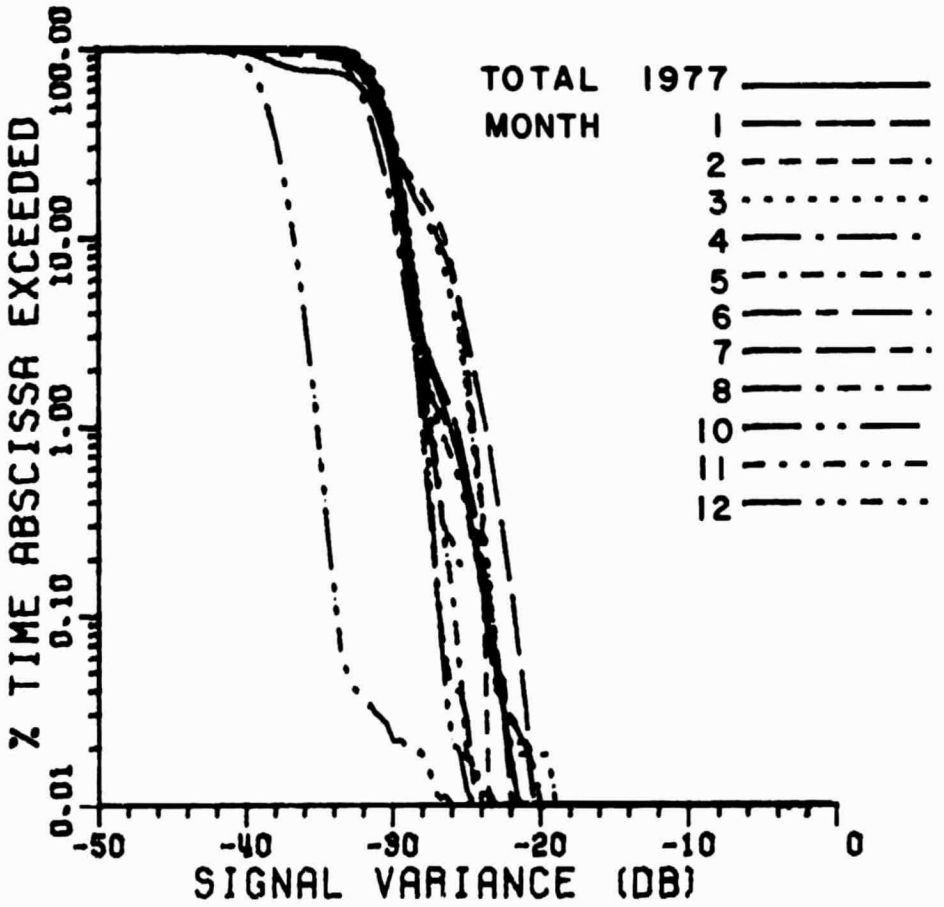

Figure 25. Monthly cumulative distributions of sum amplitude variance for January-December (except September), 1977. The solid line denotes total distribution in 1977.

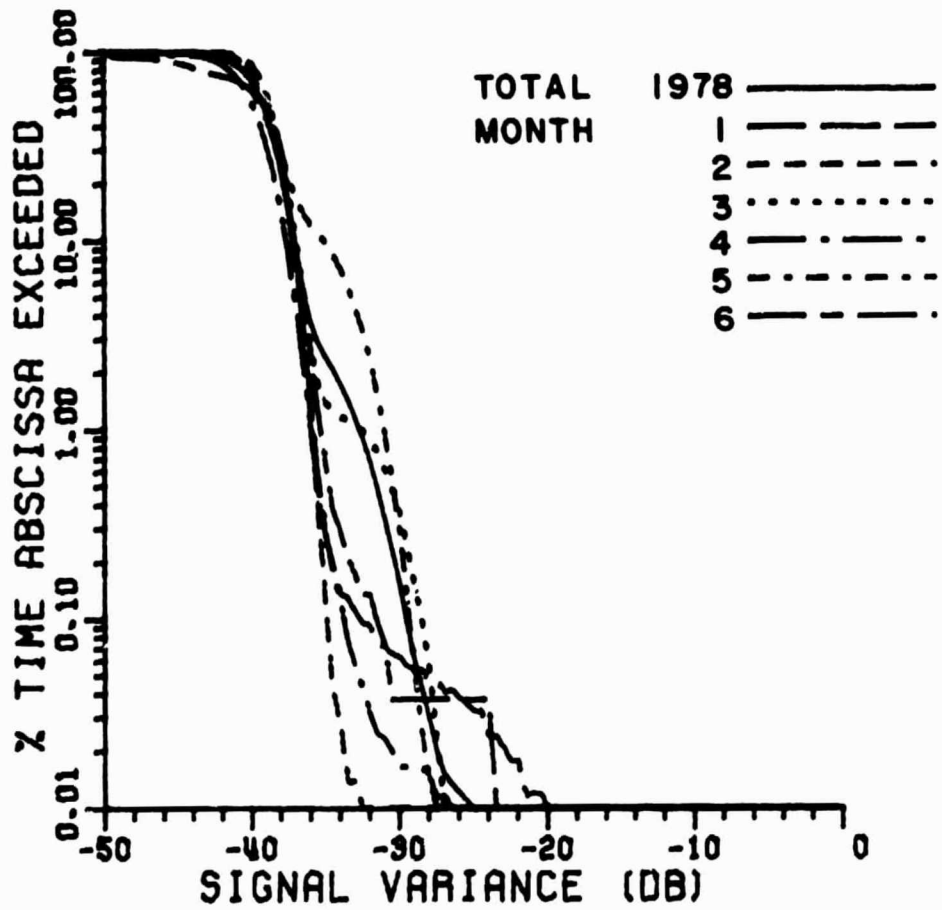

Figure 26. Cumulative distributions of sum amplitude variance for January-June, 1978. The solid line denotes the total distribution in 1978.

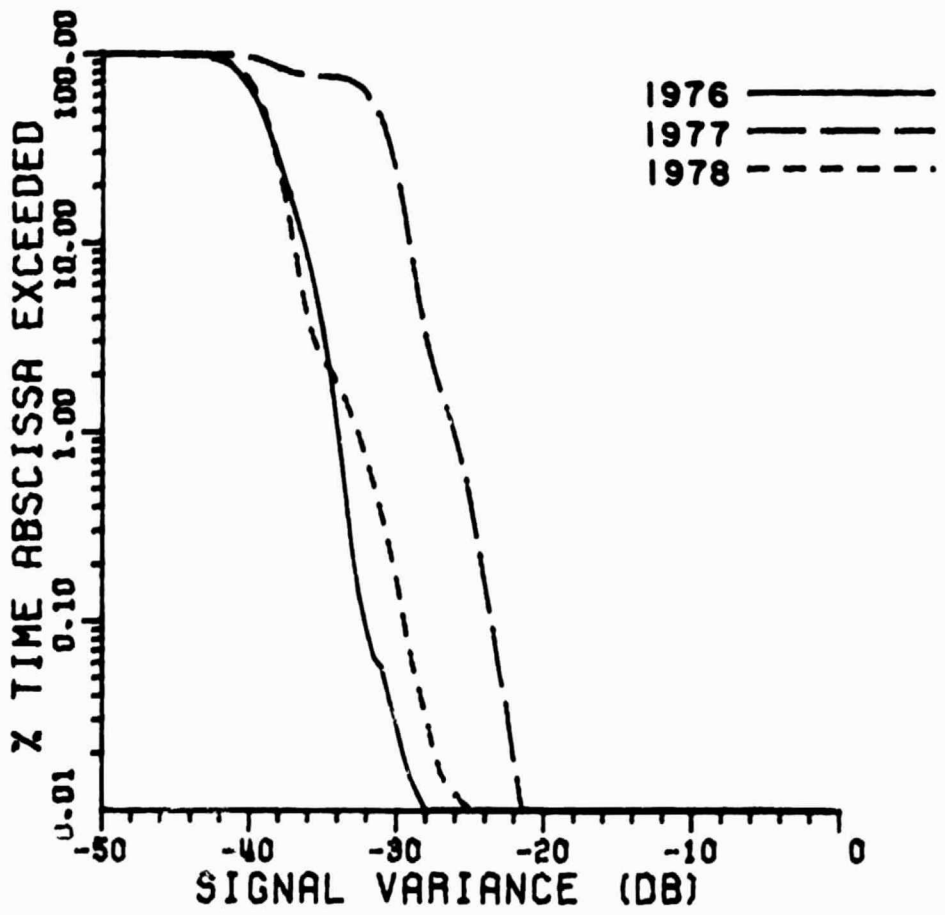

Figure 27. Cumulative distributions of sum amplitude for 1976, 1977, and 1978.

it appears that significant increases in variance do occur during fade events.

The amplitude variance for 1976, 1977, and 1978, are compared in Figure 27. Here it can be noted that the behavior in 1976 and 1978 was consistent. The variance tends to increase smoothly with decreasing percentages of time; this is probably a result of cloud scintillation which occurs much more often than rain fade events.

Differential Phase Statistics

Figure 28 displays the differential phase angle distribution for May, June, and August, 1976. Similar displays for 1977 and 1978 are presented in Figures 29 and 30, respectively. The distribution curves for May and June, 1978, should be considered the most reliable. They indicate that the differential electrical phase fluctuations exceed 30^{o} for approximately 0.01 percent of the time. This fluctuation corresponds to a 0.10^{o} change in the physical angle of arrival. The majority of curves in 1976 and 1978 tend to bend and level off for roughly 0.3 percent time of the year. The cause of this abnormal behavior is not known, but it is believed that it is not due to atmospheric effects. Furthermore, the slopes of the curves for January-November, 1977, are considerably lower than for the other months. This correlates with the increased amplitude variance observed during this period and, thus, this data period should be considered suspect. It should be noted that the remaining data are quite consistent down to percentage times from 0.1 to 1.0.

The variability of the phase fluctuations for 1976, 1977, and 1978, are described by the variance distributions shown in Figures 31-33, respectively. The minimum variance was approximated 40 dB below a square degree; and this variance increased 10 to 20 dB for 0.01 percent of the time. Again, it is noted that the phase variance during January-November, 1977, is not consistently higher than the remaining data.

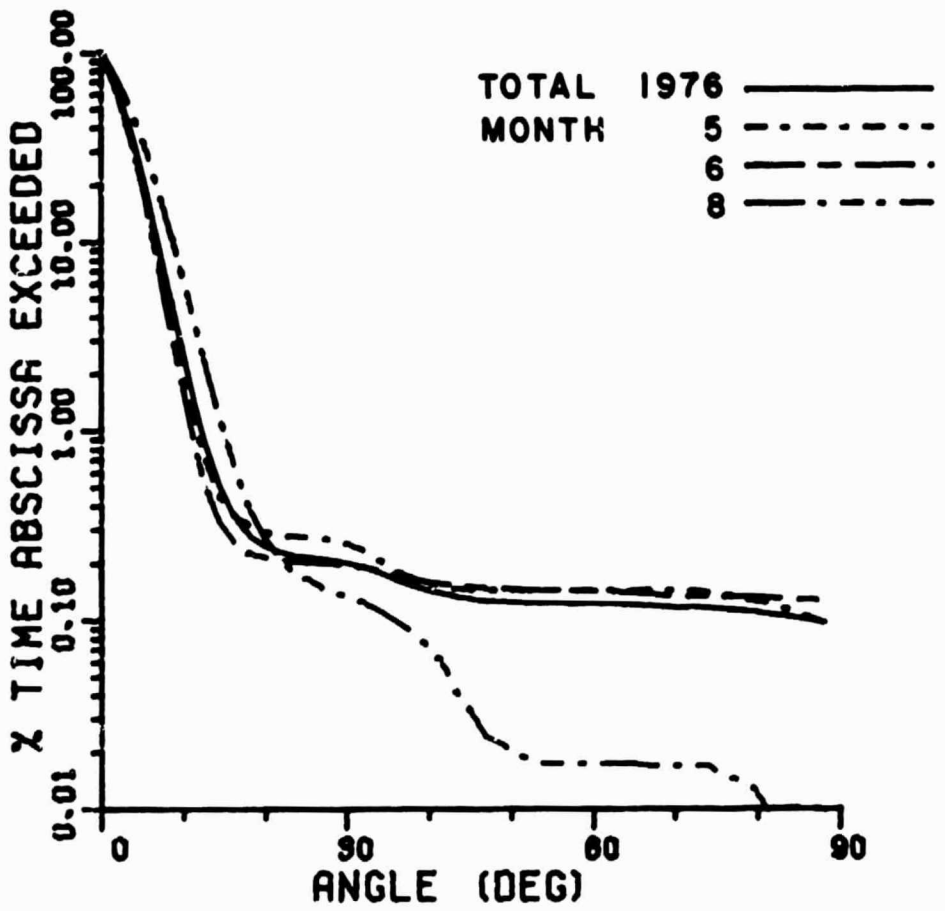

Figure 28. Cumulative distributions of differential phase for May, June, and August, 1976. The solid line denotes the total distributions in 1976.

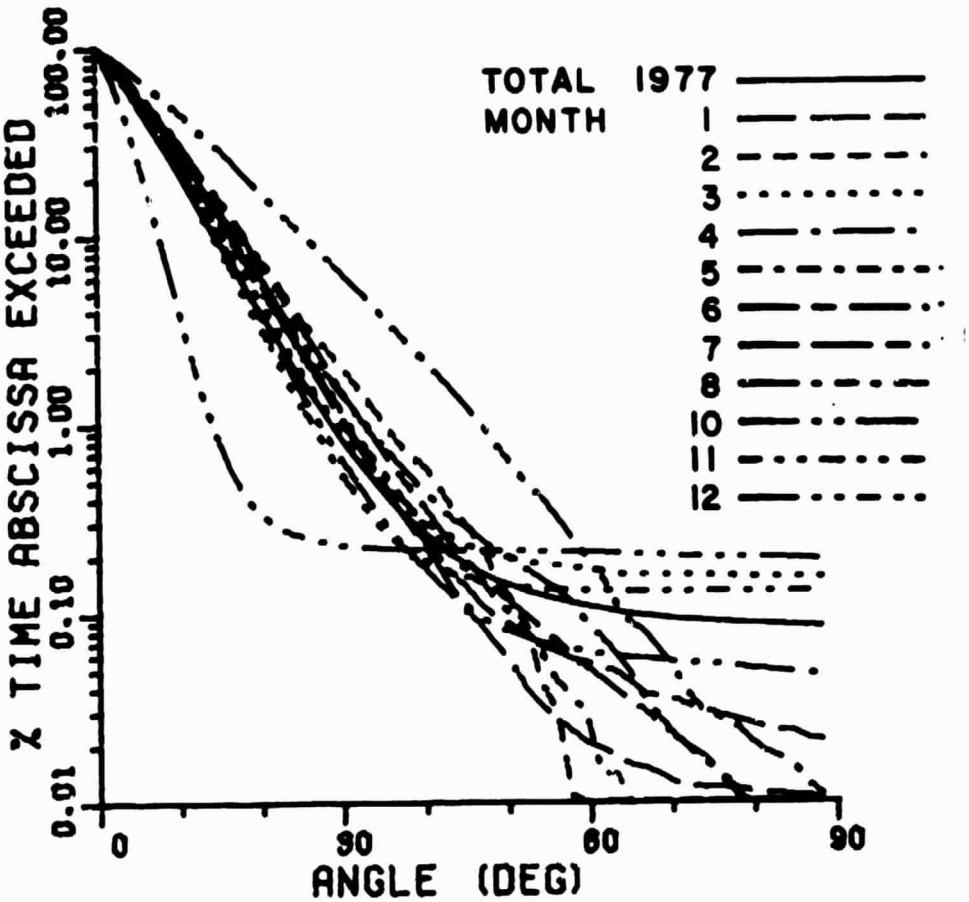

Figure 29. Cumulative distributions of differential phase for January-December (except September), 1977. The solid line denotes the total distribution in 1977.

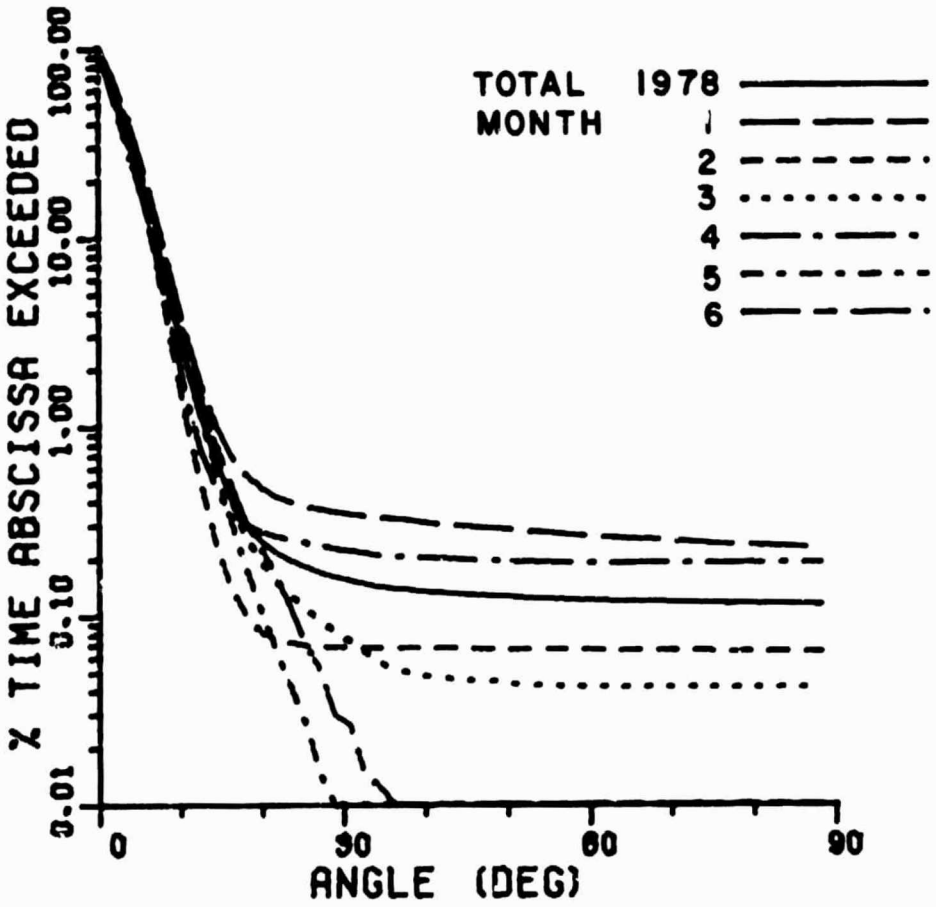

Figure 30. Cumulative distributions of differential phase for January-June, 1978. The solid line denotes the total distribution for 1978.

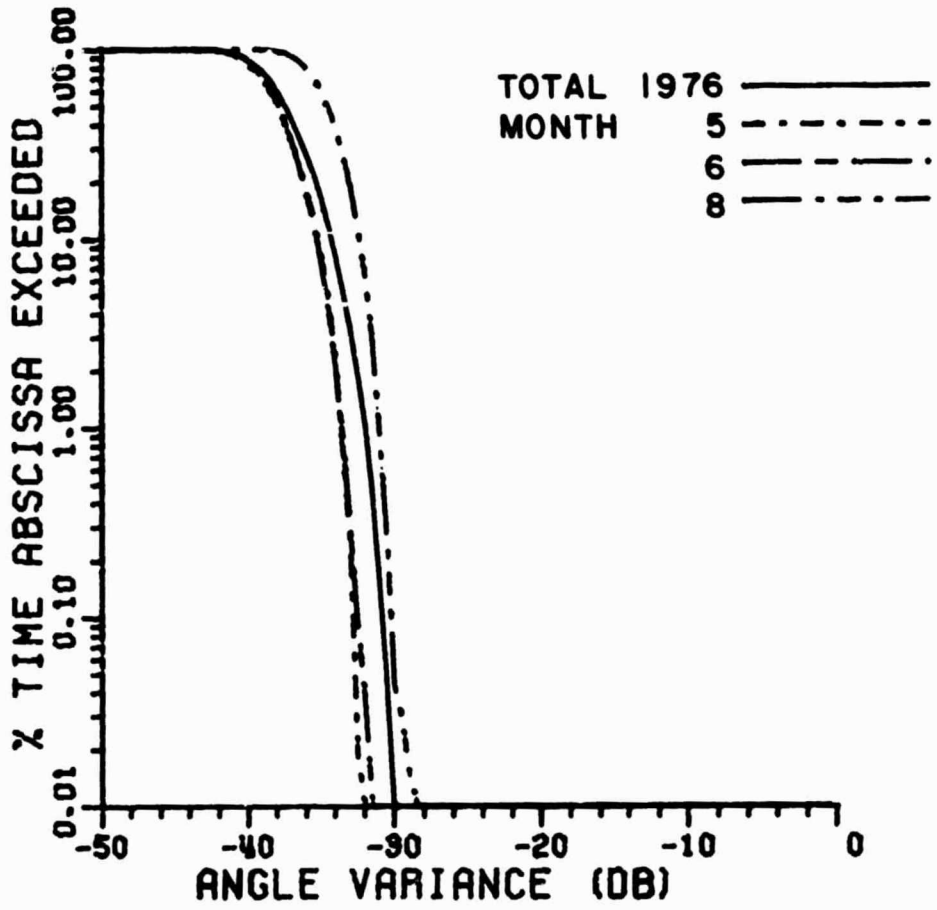

Figure 31. Cumulative distributions of differential phase variance for May, June, and August, 1976. The solid line denotes the total distribution for 1976.

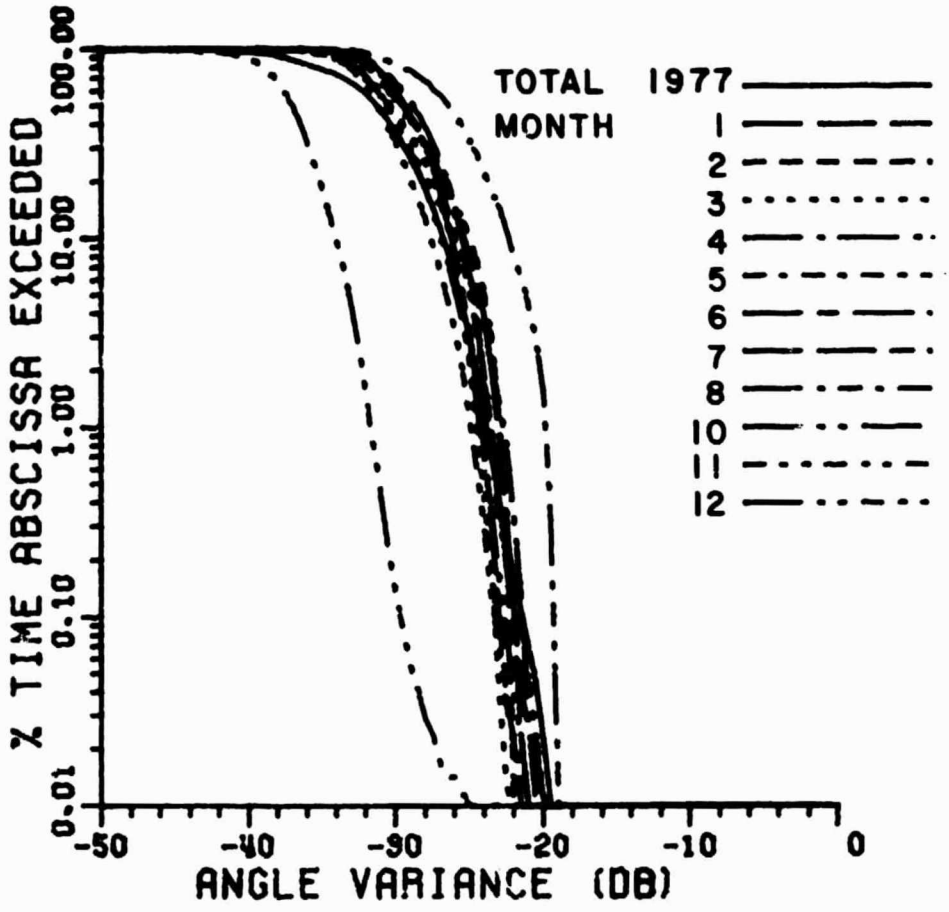

Figure 32. The cumulative distributions of differential phase variance for January-December (except September), 1977. The solid line denotes the total distribution in 1977.

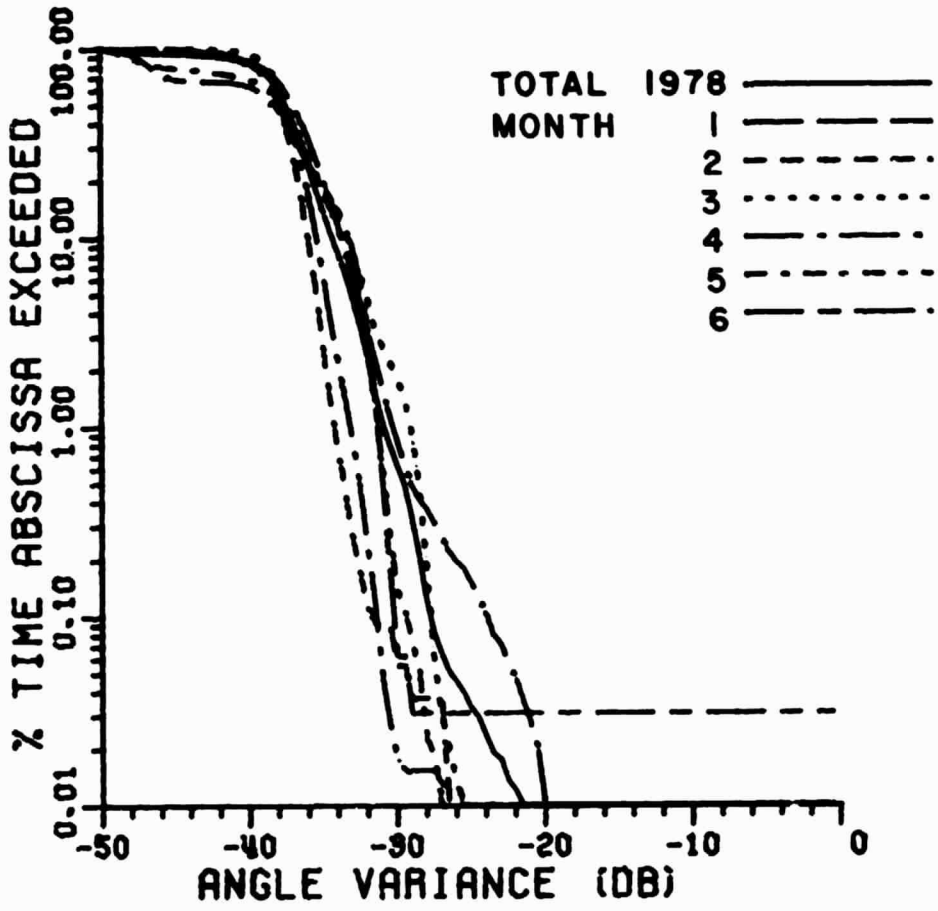

Figure 33. Cumulative distributions of differential phase variance for January-June, 1978. The solid line denotes the total distribution in 1978.

V. RAIN RATE

Rain rate distributions for the data periods are shown in Figures 34 and 35. Figure 34 shows the distributions for the data periods only, while Figure 33 shows the total annual distributions. In both cases, it can be noted that the year-to-year variability is surprisingly small. This correlates well with the consistency of the fade distributions shown in Figure 23 for these three years.

VI. DISCUSSION

The CTS 11.7 GHz angle of arrival experiment has been summarized. Analysis of the entire data set has shown that the attenuation exceeds 8 dB for 0.001 percent of the time. The apparent physical angle of arrival exceeds 0.10^{o} for 0.01 percent of the time. From the 28.56 GHz Comstar D/3 beacon measurements, which are currently underway at OSU, it is found that the physical angle of arrival exceeds 0.12^{o} for the same percentage of time. These values confirm Tatarski's result [5] that the apparent angle of arrival would be frequency independent. They also indicate that gain degradation may be evident during deep fading events for antennas having $\frac{D}{\lambda}$ on the order of 1000 or larger.

If parabolic antennas are used, one obviously cannot compensate for phase fluctuations along separated rays' paths since the various contributions collected by the fixed parabolic surface are summed directly in the feed. Therefore, one would expect to observe gain degradation when utilizing electrically large parabolic antennas. A direct gain comparison of a 60 cm and 5 m aperture at 28.56 GHz is currently underway at OSU. In this experiment, the antennas are mounted coaxially so that no decorrelation will result from spatial separation. The signals received from both antennas are switched in a manner analogous to that used in a Dicke radiometer so that any gain fluctuations in the receiver will be common to both signals.

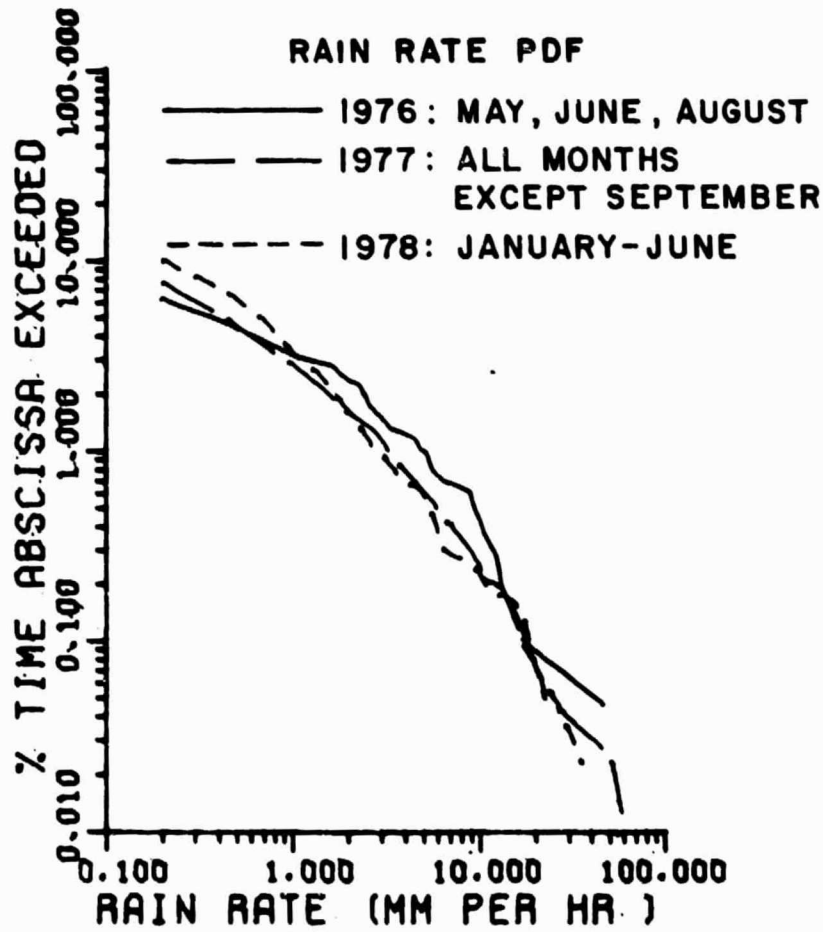

Figure 34. Rain rate distributions for the CTS 11.7 GHz angle of arrival experiment data periods.

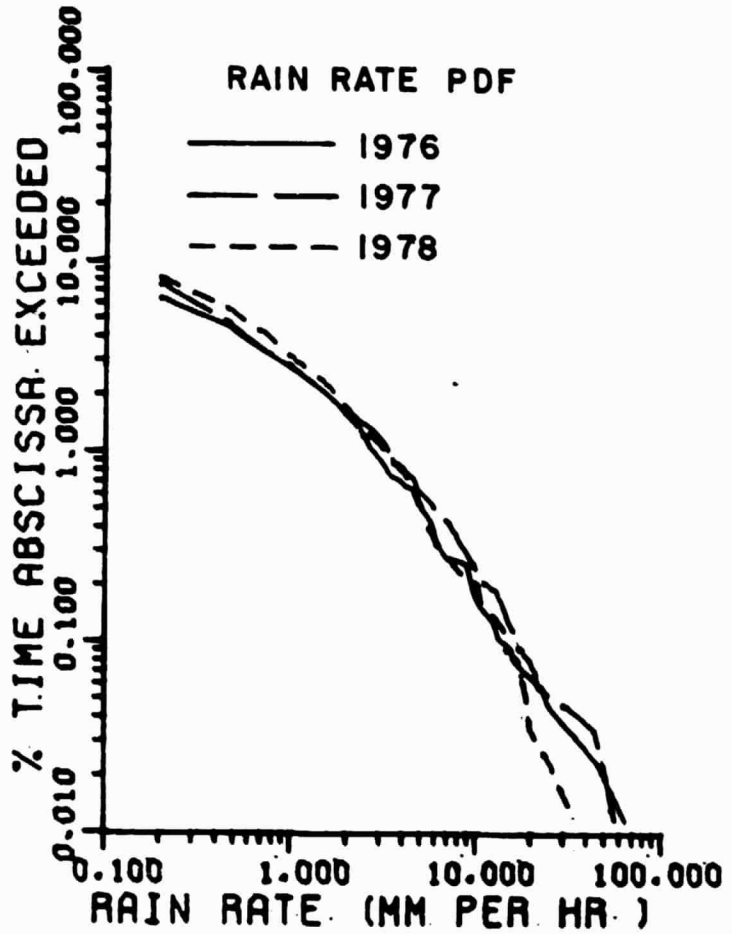

Figure 35. Rain rate distributions for 1976, 1977, and 1978.

REFERENCES

1. D.M. Theobold and D.B. Hodge, "The O.S.U. Self-Phased Array for Propagation Measurements Using the 11.7 GHz CTS Beacon," Technical Report 4299-1, November 1976, The Ohio State University ElectroScience Laboratory, Department of Electrical Engineering; prepared under Contract NAS5-22575 for NASA-Goddard Space Flight Center.

2. D.B. Hodge and D.M. Theobold, "O.S.U. Participation in the CTS Communications Link Characterization Experiment," Final Report 4299-2, December 1976, The Ohio State University ElectroScience Laboratory, Department of Electrical Engineering; prepared under Contract NAS5-22575 for NASA-Goddard Space Flight Center.

3. D.M. Theobold and D.B. Hodge, "ATS-6 Millimeter Wavelength Propagation Experiments," Report 3863-4, April 1975, The Ohio State University ElectroScience Laboratory, Department of Electrical Engineering; prepared under Contract NAS5-21983 for NASA-Goddard Space Flight Center.

4. R.A. Baxter and D.B. Hodge, "Spectral Characteristics of Earth-Space Paths at 2 and 30 GHz," Technical Report 784299-7, August 1978, The Ohio State University ElectroScience Laboratory, Department of Electrical Engineering; prepared under Contract NAS5-22575 for NASA-Goddard Space Flight Center.

5. V.J. Tatarski, "Wave Propagation in a Turbulence Medium," translated from Russian by R.A. Silverman, 285 pages, McGraw-Hill, New York, 1961.

6. T. Sukuba, T. Kokubunji, K. Funakawa, T. Kido, K. Kitamura, Y. Otsu, T. Katto, and M. Uratsuka, "Propagation Experiments of 13 GHz and 35 GHz Over the Path 80 Km," Journal of the Radio Research Laboratories, Vol. 14, No. 76 (November 1967): 249.

7. W.L. Lees, "High Resolution Measurement of Microwave Refraction on Short Tropospheric Paths," IEEE Transactions on Antennas and Propagation, V. AP-20, No. 2 (March 1972): 176.